rocscience

RS2 THEORY

PM4Sand (Version 3.1): A Sand Plasticity Model for Earthquake Engineering Applications

Table of Contents

1- Introduction

Numerical simulations of problems involving liquefaction are increasingly implemented in earthquake engineering practice. Different Constitutive models have been used fort this purpose with different level of complexities such as model base on the framework of bounding surface plasticity, kinematic hardening, etc. Dafalias and Manzari model is an example of such models that was previously developed for RS2. Each constitutive model has certain advantages and limitations that can be illustrated for potential users by documents showing the constitutive response of the model in element tests that cover a broad range of the conditions that may be important to various applications.

The PM4Sand (version 3.1) plasticity model for geotechnical earthquake engineering applications is developed in RS2 based on the work by Boulanger and Ziotopoulou (2017). The detailed formulation will be presented here. Verifications will be provided that compare the simulations results from RS2 and the results obtained from the original code developed by Boulanger and Ziotopoulou (2017). The model that is coded as a dynamic link library (DLL) for use with the commercial program FLAC 8.0 (Itasca 2016) along with the verification model files are available in https://pm4sand.engr.ucdavis.edu/pm4sand-files.

2- Model Formulation

The PM4Sand plasticity model follows the basic framework of the stress-ratio controlled, critical state compatible, bounding-surface plasticity model for sand presented by Dafalias and Manzari (2004). The model is presented in its multi-axial formulation, along with the original framework of the Dafalias-Manzari model for comparison.

2.1- Basic stress and strain terms

The basic stress and strain terms for the model are as follows. The model is based on effective stresses, with the conventional prime symbol dropped from the stress terms for convenience because all stresses are effective for the model. The stresses are represented by the tensor **σ**, the principal effective stresses σ_1, σ_2, and σ_3, the mean effective stress p, the deviatoric stress tensor **s**, and the deviatoric stress ratio tensor **r**. The present implementation was further simplified by casting the various equations and relationships in terms of the in-plane stresses only. This limits the implementation to plane-strain applications and is not correct for general cases, but it has the advantage of simplifying the implementation and improving computational speed by reducing the number of operations. The relationships between the various stress terms can be summarized as follows:

$$\boldsymbol{\sigma} = \begin{pmatrix} \sigma_{xx} & \sigma_{xy} \\ \sigma_{xy} & \sigma_{yy} \end{pmatrix} \tag{2.1}$$

$$p = \frac{\sigma_{xx} + \sigma_{yy}}{2} \tag{2.2}$$

$$\boldsymbol{s} = \boldsymbol{\sigma} - p\boldsymbol{I} = \begin{pmatrix} S_{xx} & S_{xy} \\ S_{xy} & S_{yy} \end{pmatrix} = \begin{pmatrix} \sigma_{xx} - p & \sigma_{xy} \\ \sigma_{xy} & \sigma_{yy} - p \end{pmatrix} \tag{2.3}$$

$$\boldsymbol{r} = \frac{\boldsymbol{s}}{p} = \begin{pmatrix} r_{xx} & r_{xy} \\ r_{xy} & r_{yy} \end{pmatrix} = \begin{pmatrix} \frac{\sigma_{xx} - p}{p} & \frac{\sigma_{xy}}{p} \\ \frac{\sigma_{xy}}{p} & \frac{\sigma_{yy} - p}{p} \end{pmatrix} \tag{2.4}$$

Note that the deviatoric stress and deviatoric stress ratio tensors are symmetric and traceless, and that **I** is the identity matrix.

The model strains are represented by a tensor **ε**, which can be separated into the volumetric strain ε_v and the deviatoric strain tensor **e**. The volumetric strain in plane strain is,

$$\varepsilon_v = \varepsilon_{xx} + \varepsilon_{yy} \tag{2.5}$$

and the deviatoric strain tensor is,

$$\boldsymbol{e} = \varepsilon - \frac{\varepsilon_v}{3} I = \begin{pmatrix} \varepsilon_{xx} - \frac{\varepsilon_v}{3} & \varepsilon_{xy} \\ \varepsilon_{xy} & \varepsilon_{yy} - \frac{\varepsilon_v}{3} \end{pmatrix} \tag{2.6}$$

In incremental form, the deviatoric and volumetric strain terms are decomposed into an elastic and a plastic part,

$$d\boldsymbol{e} = d\boldsymbol{e}^{el} + d\boldsymbol{e}^{pl} \tag{2.7}$$

$$d\varepsilon_v = d{\varepsilon_v}^{el} + d{\varepsilon_v}^{pl} \tag{2.8}$$

Where superscripts *el* and *pl* stand for elastic and plastic respectively.

2.2- Critical state

Dafalias and Manzari (2004) used a power relationship to approximate the curving of the critical state line that occurs over a broad range of confining stresses,

$$e_{cs} = e_o - \lambda \left(\frac{p_{cs}}{p_A}\right)^{\xi} \tag{2.9}$$

where p_{cs} = mean stress at critical state, e_{cs} = critical state void ratio, and e_o, λ, and ξ are parameters controlling the position and shape of the critical state line. The state of the sand was then described using the state parameter (Been and Jefferies 1985), which is the difference between the current void ratio (e) and the critical state void ratio (e_{cs}) at the same mean effective stress (p_{cs}).

The PM4Sand (Boulanger and Ziotopoulou, 2017) instead uses the relative state parameter index (ξR). The relative state parameter is the state parameter normalized by the difference between the maximum void ratio (e_{max}) and minimum void ratio (e_{min}) values that are used to define relative density (D_R). The relative state parameter "index" is just the relative state parameter defined using an empirical relationship for the critical state line.

$$\xi_R = D_{R,cs} - D_R \tag{2.10}$$

$$D_{R,cs} = \frac{R}{Q - \ln\left(100 \frac{p}{p_A}\right)} \tag{2.11}$$

where $D_{R,cs}$ = relative density at critical state for the current mean effective stress. The parameters Q and R are about 10 and 1.0, respectively, for quartzitic sands.

2.3- Bounding, dilatancy, and critical surfaces

The model incorporates bounding, dilatancy, and critical surfaces following the form of Dafalias and Manzari (2004). The present model simplifies the surfaces by removing the Lode angle dependency (e.g., friction angles are the same for compression or extension loading) that was included in the Dafalias-Manzari model, such that the bounding (M^b) and dilatancy (M^d) ratios can be related to the critical stress (M) ratio by the following simpler expressions.

$$M^b = M \cdot exp\left(-n^b \xi_R\right) \tag{2.12}$$

$$M^d = M \cdot exp\left(n^d \xi_R\right) \tag{2.13}$$

where n_b and n_d are parameters determining the values of M^b and M^d, respectively. For the present implementation, the mean normal stress p is taken as the average of the in-plane normal stresses (Equation 2.2), q is the difference in the major and minor principal in-plane stresses, and the relationship for M is therefore reduced to

$$M = 2 \cdot \sin\left(\phi_{cv}\right) \tag{2.14}$$

where ϕ_{cv} is the constant volume or critical state effective friction angle. The three surfaces can, for the simplifying assumptions described above, be conveniently visualized as linear lines on a q-p plot (where $q=\sigma_1-\sigma_3$) as shown in Figure 2.1 or as circular surfaces on a stress-ratio graph of r_{yy} versus r_{xy} as shown in Figure 2.2.

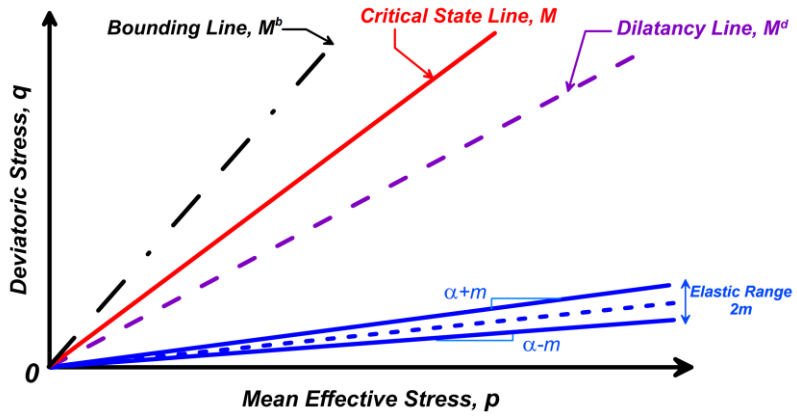

Figure 2.1. Schematic of yield, critical, dilatancy, and bounding lines in q-p space (after Dafalias & Manzari 2004)

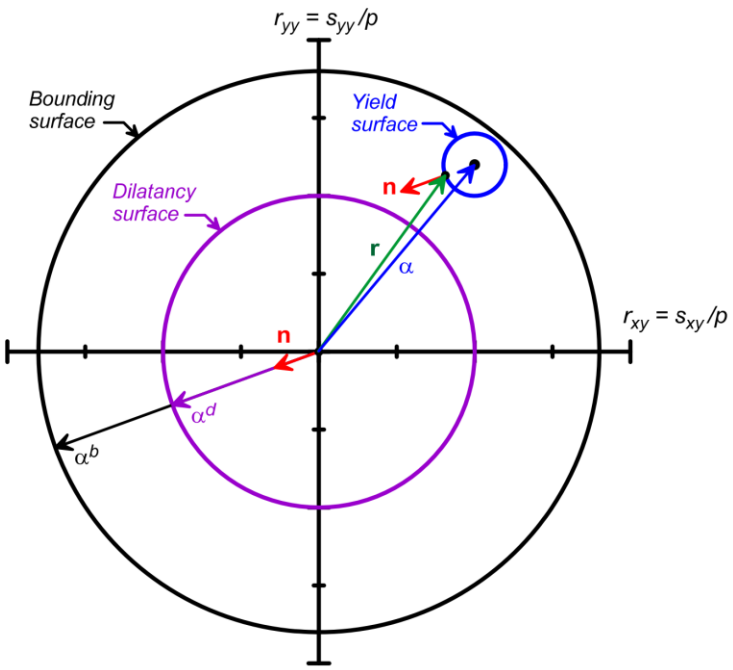

Figure 2.2. Schematic of the bounding, dilatancy, and yield surfaces on the ryy-rxy stress-ratio plane with the yield surface, normal tensor, dilatancy back stress ratio, and bounding back stress ratio

As the model is sheared toward critical state ($\xi_R = 0$), the values of M^b and M^d will both approach the value of M. Thus the bounding and dilatancy surfaces move together during shearing until they coincide with the critical state surface when the soil has reached critical state.

2.4- Yield surface and image back-stress ratio tensors

The yield surface and back-stress ratio tensor ($\boldsymbol{\alpha}$) follow those of the Dafalias-Manzari model, although their final form is considerably simplified by eliminating the dependency on Lode angle. The yield surface is a small cone in stress space, and is defined in stress terms by the following expression:

$$f = [(\boldsymbol{s} - p\boldsymbol{\alpha}) : (\boldsymbol{s} - p\boldsymbol{\alpha})]^{1/2} - \sqrt{1/2}\, pm = 0 \tag{2.15}$$

The back-stress ratio tensor $\boldsymbol{\alpha}$ defines the center of the yield surface, and the parameter m defines the radius of the cone in terms of stress ratio. The yield function can be rewritten to emphasize the role of stress ratio terms as follows,

$$f = \sqrt{(\boldsymbol{r} - \boldsymbol{\alpha}) : (\boldsymbol{r} - \boldsymbol{\alpha})} - \sqrt{1/2}\, m = 0 \tag{2.16}$$

The yield function can then be visualized as related to the distance between the stress ratio **r** and the back-stress ratio $\boldsymbol{\alpha}$, as illustrated in Figure 2.2.

The bounding surface formulation now requires that bounding and dilatancy stress ratio tensors be defined. Dafalias and Manzari (2004) showed that it is more convenient to track back-stress ratios and to similarly

define bounding and dilatancy surfaces in terms of back-stress ratios. An image back-stress ratio tensor for the bounding surface ($\boldsymbol{\alpha}^b$) is defined as,

$$\boldsymbol{\alpha}^b = \sqrt{1/2}\,[M^b - m]\boldsymbol{n} \tag{2.17}$$

where the tensor **n** is normal to the yield surface. An image back-stress ratio tensor for the dilatancy surface ($\boldsymbol{\alpha}^d$) is similarly defined as,

$$\boldsymbol{\alpha}^d = \sqrt{1/2}\,[M^d - m]\boldsymbol{n} \tag{2.18}$$

The computation of constitutive responses can now be more conveniently expressed in terms of back-stress ratios rather than in terms of stress ratios, as noted by Dafalias and Manzari (2004).

2.5- Stress reversal and initial back-stress ratio tensors

The bounding surface formulation keeps track of the initial back-stress ratio ($\boldsymbol{\alpha}_{in}$) and uses it in the computation of the plastic modulus K_p. This tracking of one instance in loading history is essentially a first-order method for tracking loading history. A reversal in loading direction is then identified, following traditional bounding surface practice, whenever

$$(\alpha - a_{in}) : \boldsymbol{n} < 0 \tag{2.19}$$

A reversal causes the current stress ratio to become the initial stress ratio for subsequent loading. Small cycles of load reversal can reset the initial stress ratio and cause the plastic modulus K_p to increase accordingly, in which case the stress-strain response becomes overly stiff after a small load reversal. This is a well-known problem in bounding surface formulations for which various approaches offer different advantages and disadvantages.

The model presented herein tracks an initial back-stress ratio and a previous initial back-stress ratio ($\boldsymbol{\alpha}_{in}^p$), as illustrated in Figure 2.3a. When a reversal occurs, the previous initial back-stress ratio is updated to the initial back stress ratio, and the initial back-stress ratio is updated to the current back-stress ratio.

In addition, the model tracks an apparent initial back-stress ratio tensor ($\boldsymbol{\alpha}_{in}^{app}$) as schematically illustrated in Figure 2.3b. The schematic in Figure 2.3b is similar to that of Figure 2.3a, except that the most recent loading reversals correspond to a small unload-reload cycle on an otherwise positive loading branch. The components of $\boldsymbol{\alpha}_{in}^{app}$ are taken as: (i) for positive loading directions, the minimum value they have ever had, but no smaller than zero, and (ii) for negative loading directions, the maximum value they have ever had, but no greater than zero. The use of $\boldsymbol{\alpha}_{in}^{app}$ helps avoid the over-stiffening of the stress-strain response following small unload-reload cycles along an otherwise monotonically increasing branch of loading, without having to track the loading history through many cycles of load reversals.

The computation of K_p utilizes the values of $\boldsymbol{\alpha}_{in}^{app}$, $\boldsymbol{\alpha}_{in}^{true}$, and $\boldsymbol{\alpha}_{in}^{p}$, as defined in Figure 2.3b, to better approximate the stress-strain response during an unload-reload cycle. For the last positive loading branch in this figure, the value of K_p is initially most strongly controlled (inversely) by the distance ($\boldsymbol{\alpha}$ - $\boldsymbol{\alpha}_{in}^{true}$):n, such that the stiffness is initially large. As positive loading continues, the progressive reduction in K_p becomes increasingly dependent on $\boldsymbol{\alpha}_{in}^{app}$ as well. Once the positive loading exceeds the previous reversal point, the value of K_p becomes solely dependent on the distance ($\boldsymbol{\alpha}$ - $\boldsymbol{\alpha}_{in}^{app}$):n. Thus, the computation of K_p has the following dependencies:

$$if\left(\boldsymbol{\alpha}-\boldsymbol{\alpha}_{in}^{p}\right):\boldsymbol{n}<0 \Longrightarrow K_p = f\left(\boldsymbol{\alpha}_{in}^{true},\boldsymbol{\alpha}_{in}^{app}\right)$$
$$else \qquad \Longrightarrow K_p = f\left(\boldsymbol{\alpha}_{in}^{app}\right) \tag{2.20}$$

The equations relating K_p to these back-stress ratios are given later in section 2.7.

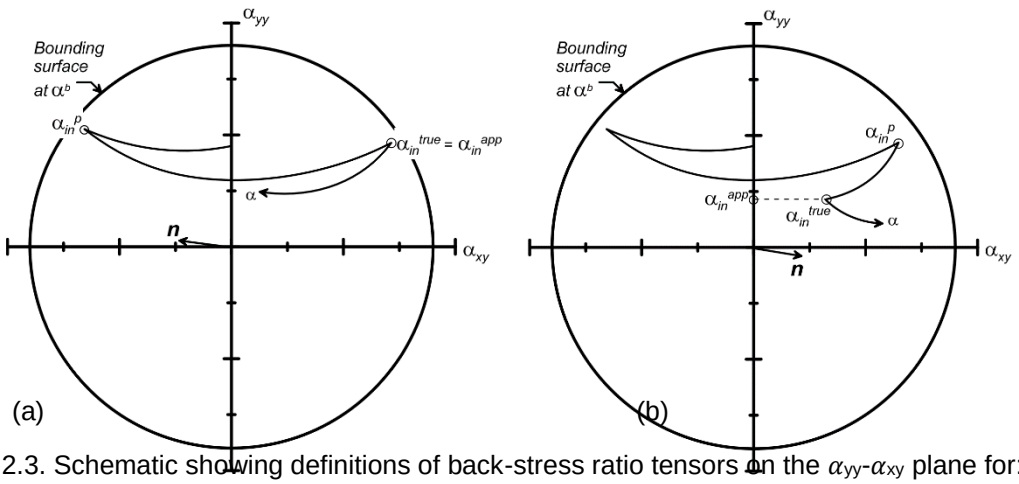

Figure 2.3. Schematic showing definitions of back-stress ratio tensors on the α_{yy}-α_{xy} plane for: (a) a loading history with reversals in the sign of the shear stress ratios, and (b) a loading history with a recent loading reversal that does not involve reversal of the sign of the shear stress ratios

The impact of the above logic for defining $\boldsymbol{\alpha}_{in}$ on stress-strain responses is demonstrated in Figure 2.4 showing α_{xy} versus shear strain γ computed for two different drained DSS loading simulations. For these two examples, the reloading stiffness of the current loading branch (green line) is initially large because K_p is initially computed based on $\boldsymbol{\alpha}_{in} = \boldsymbol{\alpha}_{in}^{true}$. As the loading exceeds $\boldsymbol{\alpha}_{in}^{p}$, the loading stiffness becomes much softer because K_p is now computed based on $\boldsymbol{\alpha}_{in} = \boldsymbol{\alpha}_{in}^{app}$.

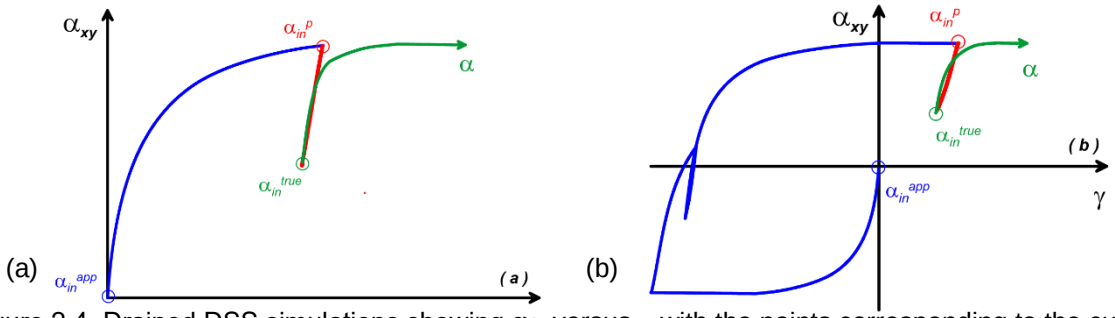

Figure 2.4. Drained DSS simulations showing α_{xy} versus γ with the points corresponding to the current back-stress ratio α, the apparent initial back-stress ratio α_{inapp}, the true initial back-stress ratio α_{intrue}, and the previous initial back-stress ratio α_{inp} for: (a) monotonic shearing with one intermediate unload-reload cycle, and (b) a more general sequence of cyclic loading.

2.6- Elastic strains and moduli

The elastic deviatoric strain and elastic volumetric strain increments are computed as:

$$d\boldsymbol{e}^{el} = \frac{d\boldsymbol{s}}{2G} \tag{2.21}$$
(2.22)

$$d\varepsilon_v^{el} = \frac{dp}{K}$$

where G is the elastic shear modulus and K is the elastic bulk modulus. The elastic shear modulus in the model presented herein is dependent on the mean effective stress according to,

$$G = G_o p_A \left(\frac{p}{p_A}\right)^{1/2} C_{SR} \tag{2.23}$$

where G_o is a constant, p_A is the atmospheric pressure (101.3 kPa), and CSR is factor that accounts for stress ratio effects.

Dafalias and Manzari (2004) had included the dependence of G on void ratio. This aspect was not included in PM4ANS model because: (1) the effects of void ratio changes on G are small relative to those of confining stress, (2) the value of G_o is more strongly affected by environmental factors such as cementation and ageing, and (3) the calibration of G to in-situ shear wave velocity data requires only one constant (G_o) rather than two (G_o and e).

Yu and Richart (1984) showed that the small-strain elastic shear modulus of sand is dependent on the stress ratio and stress ratio history. The effect of stress ratio was shown to generally be less than about 10% when the ratio of major to minor principal effective stresses is less than about 2.5, but to also increase to about 20-30% at higher principal stress ratios. They also showed that stress ratio history caused a reduction in the small-strain elastic shear modulus when the maximum previous stress ratio was greater than the current stress ratio. The effect of stress ratio and stress ratio history on the elastic shear modulus was approximately accounted for in the present model by the factor C_{SR}. The following equation for C_{SR} is similar in form to that used by Yu and Richart (1984) to represent stress ratio effects, except that it uses stress ratio terms consistent with the present model,

$$C_{SR} = 1 - C_{SR,o} \cdot \left(\frac{M}{M^b}\right)^{m_{SR}} \tag{2.24}$$

The above equation approximates Yu and Richart's (1984) results for stress ratio effects when $C_{SR,0}$ = 0.3 and m_{SR} = 2. The effects of stress ratio history would cause further reductions, and is more complicated to represent. The calibration examples presented later in this report worked well with $C_{SR,0}$ = 0.5 and m_{SR} = 4, which keeps the effect of stress ratio on elastic modulus small at small stress ratios, but lets the effect increase to a 60% reduction when the stress ratio is on the bounding surface.

The elastic bulk modulus is related to the shear modulus through the Poisson's ratio as,

$$K = \frac{2(1+v)}{3(1-2v)} G \tag{2.25}$$

as was done by Dafalias and Manzari (2004).

2.7- Plastic components without fabric effects

Loading index

The loading index (L) is used to compute the plastic component of the volumetric strain increment and the plastic deviatoric strain increment tensor as,

$$d\varepsilon_v^{pl} = \langle L \rangle D \tag{2.26}$$

(2.27)

$$d\boldsymbol{e}^{pl} = \langle L \rangle \boldsymbol{R}'$$

where D is the dilatancy, **R** is the direction of $d\boldsymbol{\varepsilon}^{pl}$, **R′** is the deviatoric component of **R**, and <> are MacCauley brackets that set negative values to zero [i.e.,<L> = L if L ≥ 0, and <L> = 0 if L < 0]. The tensor **R** for the assumption of no Lode angle dependency is,

$$\boldsymbol{R} = \boldsymbol{n} + \frac{1}{3} D\boldsymbol{I} \tag{2.28}$$

where **n** is the unit normal to the yield surface (Figure 2.2). Note that the assumption of no Lode angle dependency also means that **R′** = **n**. The dilatancy D relates the incremental plastic volumetric strain to the incremental plastic deviatoric strain,

$$D = \frac{d\varepsilon_v^{pl}}{|d\boldsymbol{e}^{pl}|} \tag{2.29}$$

The dilatancy D can be also related to the conventional engineering shear strain in this plane strain approximation, as

$$D = \frac{d\varepsilon_v^{pl}}{\sqrt{1/2}\,|d\gamma^{pl}|} \tag{2.30}$$

The loading index, as derived in Dafalias and Manzari (2004) is,

$$L = \frac{1}{K_p}\frac{\partial f}{\partial \boldsymbol{\sigma}} : d\boldsymbol{\sigma} = \frac{1}{K_p}[\boldsymbol{n} : d\boldsymbol{s} - \boldsymbol{n} : \boldsymbol{r} dp]$$
$$L = \frac{2G\boldsymbol{n} : d\boldsymbol{e} - \boldsymbol{n} : \boldsymbol{r} K d\varepsilon_v}{K_p + 2G - KD\boldsymbol{n} : \boldsymbol{r}} \tag{2.31}$$

The stress increment for an imposed strain increment can then be computed as,

$$d\sigma = 2Gd\boldsymbol{e} + Kd\varepsilon_v \boldsymbol{I} - \langle L \rangle (2G\boldsymbol{n} + KD\boldsymbol{I}) \tag{2.32}$$

Hardening and the update of the back-stress ratio

Updating of the back-stress ratio is dependent on the hardening aspects of the model. Dafalias and Manzari (2004) updated the back-stress ratio according to bounding surface practice as,

$$d\boldsymbol{\alpha} = \langle L \rangle \left(\frac{2}{3}\right) h(\boldsymbol{\alpha}^b - \boldsymbol{\alpha}) \tag{2.33}$$

where h is the hardening coefficient. The factor of 2/3 was included for convenience so that model constants would be the same in triaxial and multi-axial derivations. They subsequently showed that the consistency condition $\delta f=0$ was satisfied when the plastic modulus K_p was related to the hardening coefficient as,

$$K_p = \frac{2}{3} p \cdot h \cdot (\boldsymbol{\alpha}^b - \boldsymbol{\alpha}) : \boldsymbol{n} \tag{2.34}$$

This expression can be rearranged so as to show that the consistency equation can be satisfied by expressing the hardening coefficient as,

$$h = \frac{3}{2} \cdot \frac{K_p}{p \cdot (\boldsymbol{\alpha}^b - \boldsymbol{\alpha}) : \boldsymbol{n}} \tag{2.35}$$

The relationship for the plastic modulus can subsequently take a range of forms, provided that the hardening coefficient and updating of the back-stress ratio follow the above expressions.

Plastic modulus

The plastic modulus in the multi-axial generalized form of Dafalias and Manzari (2004), after substituting in their expression for the hardening coefficient, can be expressed as,

$$K_p = \frac{2}{3} G \cdot h_o \cdot \left[\frac{1+e}{(2.97-e)^2} \cdot (1 - C_h e) \right] \cdot \frac{(\boldsymbol{\alpha}^b - \boldsymbol{\alpha}) : \boldsymbol{n}}{(\boldsymbol{\alpha} - \boldsymbol{\alpha}_{in}) : \boldsymbol{n}} \tag{2.36}$$

where h_o and C_h are scalar parameters and e is the void ratio. Setting aside the secondary influence of void ratio, this form illustrates that K_p is proportional to G, proportional to the distance of the backstress ratio to the bounding back-stress ratio, and inversely proportional to the distance of the backstress ratio from the initial back-stress ratio.

The plastic modulus relationship was revised in the model presented herein to provide an improved approximation of empirical relationships for secant shear modulus and equivalent damping ratios during drained strain-controlled cyclic loading. The plastic modulus is computed as,

$$K_p = G \cdot h_o \cdot \frac{[(\boldsymbol{\alpha}^b - \boldsymbol{\alpha}) : \boldsymbol{n}]^{0.5}}{\left[exp\left[(\boldsymbol{\alpha} - \boldsymbol{\alpha}_{in}^{app}) : \boldsymbol{n} \right] - 1 \right] + C_{\gamma 1}} C_{rev} \tag{2.37}$$

$$C_{rev} = \frac{(\boldsymbol{\alpha} - \boldsymbol{\alpha}_{in}^{app}) : \boldsymbol{n}}{(\boldsymbol{\alpha} - \boldsymbol{\alpha}_{in}^{true}) : \boldsymbol{n}} \quad for \quad (\boldsymbol{\alpha} - \boldsymbol{\alpha}_{in}^{p}) : \boldsymbol{n} \leq \boldsymbol{0} \tag{2.38}$$

$$= 1 \; otherwise$$

The factor C_{rev} accounts for the effect of unload-reload cycles as discussed in Section 2.5 and illustrated in Figure 2.4. The constant $C_{\gamma 1}$ in the denominator serves to avoid division by zero and has a slight effect on the nonlinearity and damping at small shear strains. If $C_{\gamma 1} = 0$, then the value of K_p will be infinite at the start of a loading cycle because $(\boldsymbol{\alpha}-\boldsymbol{\alpha}_{in}):\boldsymbol{n}$ will also be zero. In that case, nonlinearity will become noticeable only after $(\boldsymbol{\alpha}-\boldsymbol{\alpha}_{in}):\boldsymbol{n}$ becomes large enough to reduce K_p closer to the value of G (e.g., K_p/G closer to 100 or 200). Setting the value of $C_{\gamma 1} = h_o/200$ produces a reasonable response as will be demonstrated later with examples of modulus reduction and equivalent damping ratios. For stress ratios outside the bounding surface [i.e., loose-of-critical states with $(\boldsymbol{\alpha}^b - \boldsymbol{\alpha}):\boldsymbol{n} < 0$], the plastic modulus is set to zero rather than allowing for negative values. This restriction on the plastic modulus improved numerical stability while having little effect on computed stress-strain responses. The plastic modulus is further modified for the effects of fabric and fabric history, as described in a later section.

Plastic volumetric strains - Dilation

Plastic volumetric strains are related to plastic deviatoric strains through the dilatancy D (Equations 2.29 and 2.30), which is computed in the Dafalias and Manzari (2004) model and the base component of the model presented herein (with additional fabric effects described in a later section) as,

$$D = A_{do} \cdot \left[(\boldsymbol{\alpha}_\theta^d - \boldsymbol{\alpha}) : \boldsymbol{n} \right] \tag{2.39}$$

Note that dilation (increasing void ratio) occurs whenever the term $(\boldsymbol{\alpha}^d\text{-}\boldsymbol{\alpha}):\mathbf{n}$ is less than zero whereas contraction (decreasing void ratio) occurs when it is positive.

The constant A_{do} in this relationship can be related to the dilatancy relationship proposed by Bolton (1986), which follows from the work of Rowe (1962), through the following sequence of steps. Bolton showed that the difference between peak and constant volume friction angles could be approximated as,

$$\phi_{pk} - \phi_{cv} = -0.8\psi \tag{2.40}$$

with

$$\psi = \tan^{-1}\left(\frac{d\varepsilon_v^{pl}}{|d\gamma^{pl}|}\right) \tag{2.41}$$

Since $\psi \approx \tan(\psi)$ for ψ less than about 0.35 radians (20 degrees), the difference between peak and constant volume friction angles (in radians) can be approximated as,

$$\phi_{pk} - \phi_{cv} = -0.8\frac{d\varepsilon_v^{pl}}{|d\gamma^{pl}|} = -0.8\sqrt{\frac{1}{2}D} \tag{2.42}$$

The peak friction angle is mobilized at the bounding surface, so this can be written as,

$$\begin{aligned}\phi_{pk} - \phi_{cv} &= -0.8\sqrt{\frac{1}{2}}A_{do}\cdot[(\boldsymbol{\alpha}^d - \boldsymbol{\alpha}):\boldsymbol{n}] \\ \phi_{pk} - \phi_{cv} &= -0.8\sqrt{\frac{1}{2}}A_{do}\cdot\left[\left(\frac{M^d}{\sqrt{2}}\boldsymbol{n} - \frac{M^b}{\sqrt{2}}\boldsymbol{n}\right):\boldsymbol{n}\right]\end{aligned} \tag{2.43}$$

The term $\mathbf{n}:\mathbf{n}$ is equal to unity, and the values of ϕpk and ϕcv (again in radians) can be replaced with expressions in terms of M^b and M as,

$$\sin^{-1}\left(\frac{M^b}{2}\right) - \sin^{-1}\left(\frac{M}{2}\right) = 0.4A_{do}\cdot[M^b - M^d] \tag{2.44}$$

This expression can then be rearranged to solve for A_{do} as,

$$A_{do} = \frac{1}{0.4}\frac{\sin^{-1}\left(\frac{M^b}{2}\right) - \sin^{-1}\left(\frac{M}{2}\right)}{M^b - M^d} \tag{2.45}$$

where the angles returned by the $\sin^{-1}$ functions are in radians.

The parameter A_{do} should thus be chosen to be consistent with the n^d and n^b terms that control M^b, and M^d. For example, setting the parameters n^b and n^d equal to 0.5 and 0.1, respectively, results in A_{do} varying from 1.26 for ξ_R = -0.1 to 1.45 for ξ_R = -0.7. A default value for A_{do} is computed based on the above expression using the conditions at the time of model initialization in FLAC (as described in a later section). If an alternative value for A_{do} is manually input as a property of the model, then the default value will be deactivated.

Alternatively, the stress ratio terms can be replaced with friction angles (in radians) as follows,

$$\begin{aligned}\phi_{pk} - \phi_{cv} &= 0.4A_{do}\cdot[M^b - M^d] \\ \phi_{pk} - \phi_{cv} &= 0.4A_{do}\cdot\left[Mexp\left(-n^b\xi_R\right) - Mexp\left(n^d\xi_R\right)\right]\end{aligned} \tag{2.46}$$

$$\phi_{pk} - \phi_{cv} = 0.4A_{do} \cdot \left[2\sin\left(\phi_{pk}\right) - 2\sin\left(\phi_d\right)\right]$$

$$\phi_{pk} - \phi_{cv} = 0.8A_{do} \cdot \left[\sin\left(\phi_{pk}\right) - \sin\left(\phi_d\right)\right]$$

The sine terms can be replaced with Taylor series, which are quite accurate with just the first two terms as,

$$\sin(\phi) = \frac{(\phi)^3}{3!} \tag{2.47}$$

Substituting the Taylor series in the above equation gives,

$$\phi_{pk} - \phi_{cv} = 0.8A_{do} \cdot \left[\left(\phi_{pk} - \frac{\left(\phi_{pk}\right)^3}{3!}\right) - \left(\phi_d - \frac{\left(\phi_d\right)^3}{3!}\right)\right] \tag{2.48}$$

The parameter A_{do} can then be solved for as,

$$A_{do} = \frac{\phi_{pk} - \phi_{cv}}{0.8\left[\phi_{pk} - \phi_d - \frac{\left(\phi_{pk}\right)^3 - \left(\phi_d\right)^3}{6}\right]} \tag{2.49}$$

where the friction angles in the above expression are in radians. This expression provides an alternative view of how the parameter A_{do} relates to friction angles for a given set of n^b and n^d terms that control ϕ_{pk} and ϕ_d, respectively. For example, consider the case with the parameters n^b and n^d equal to 0.5 and 0.1, respectively, and assuming ϕ_{cv} = 33 degrees. For ξ_R = -0.1, we would obtain ϕ_d = 32.6 degrees, ϕ_{pk} = 34.9 degrees, and A_{do} = 1.26. For ξ_R = -0.7, we would obtain ϕ_d = 30.5 degrees, ϕ_{pk} = 50.6 degrees, and A_{do} = 1.45.

Plastic volumetric strains - Contraction

Plastic volumetric strains during contraction (i.e., whenever $(\boldsymbol{\alpha}^d\text{-}\boldsymbol{\alpha}):\mathbf{n}$ is greater than zero) are computed in the Dafalias and Manzari (2004) model using the same expression as used for dilatancy,

$$D = A_{do} \cdot \left[\left(\boldsymbol{\alpha}_\theta^d - \boldsymbol{\alpha}\right):\boldsymbol{n}\right] \tag{2.50}$$

The use of this expression was found to limit the ability of the model to approximate a number of important loading responses; e.g., it greatly overestimated the slope of the cyclic resistance ratio (CRR) versus number of equivalent uniform loading cycles for undrained cyclic element tests.

Plastic volumetric strains during contraction for the model presented herein are computed using the following expression,

$$D = \mathrm{A}_{dc} \cdot \left[\left(\boldsymbol{\alpha} - \boldsymbol{\alpha}_{\boldsymbol{in}}^{\boldsymbol{app}}\right):\boldsymbol{n} + C_{in}\right]^2 \frac{\left(\boldsymbol{\alpha}^d - \boldsymbol{\alpha}\right):\boldsymbol{n}}{\left(\boldsymbol{\alpha}^d - \boldsymbol{\alpha}\right):\boldsymbol{n} + C_D} \tag{2.51}$$

$$A_{dc} = \frac{\mathrm{A}_{do}}{h_p} \tag{2.52}$$

The various forms in the above relationships were developed to improve different aspects of the calibrated model's performance. The value of D was set proportional to the square of $((\boldsymbol{\alpha}\text{-}\boldsymbol{\alpha}^{in}):\mathbf{n} + C_{in})$ to improve the slope of the relationship between CRR and number of uniform loading cycles. The Cin term depends on fabric and is described in a later section along with other modifications to the above expression for the

effects of fabric and fabric history. The inclusion of the term C_{in} improves the stress paths for undrained cyclic loading and the volumetric strain response during drained cyclic loading; Inclusion of this constant enables some volumetric strain to develop early in the unloading from a point outside the dilatancy surface (as described later). The remaining terms on the right hand side of the equation were chosen to be close to unity over most of the loading range, while ensuring that D smoothly goes to zero as $\boldsymbol{\alpha}$ approaches $\boldsymbol{\alpha}^d$; reasonable results were obtained using a C_D value of 0.10.

The parameter A_{dc} for contraction was related to the value of A_{do} for dilation by dividing it by a parameter hp that can be varied during the calibration process to obtain desired cyclic resistance ratios. The effect of confining stress on cyclic loading behavior was then conveniently incorporated by making h_p depend on ξ_R, with the following form chosen so that the model produces results consistent with the design K_σ relationships.

$$h_p = h_{po}\, exp\left(-0.7 + 7.0\left(0.5 - \xi_R\right)^2\right)\ for\ \xi_R \le 0.5 \tag{2.53}$$

$$h_p = h_{po}\, exp(-0.7)\ for\ \xi_R > 0.5 \tag{2.54}$$

Thus, the scalar constant h_{po} provides a linear scaling of contraction rates while the functional form of the remaining portion in Equations (2.53) and (2.54) is what controls the effect of overburden stress on CRR. Once the other input parameters have been selected, the constant h_{po} can be calibrated to arrive at a desired cyclic resistance ratio.

A upper limit was imposed on the contraction rate, with the limiting value computed as,

$$D \le 1.5 \cdot A_{do}\, \frac{(\boldsymbol{\alpha}^d - \boldsymbol{\alpha}) : \boldsymbol{n}}{(\boldsymbol{\alpha}^d - \boldsymbol{\alpha}) : \boldsymbol{n} + C_D} \tag{2.55}$$

This limit prevented numerical issues that were encountered with excessively large contraction rates. It does not appear to have limited the ability of the model to recreate realistic contraction rates as illustrated in the calibration examples shown later.

2.8- Fabric effects

Dafalias and Manzari (2004) introduced a fabric-dilatancy tensor (**z**) that could be used to account for the effects of prior straining. Their fabric tensor (**z**) evolved in response to plastic volumetric dilation strains, according to,

$$dz = -c_z \langle -d\varepsilon_v^{pl} \rangle (z_{max}\boldsymbol{n} + \boldsymbol{z}) \tag{2.56}$$

where the parameter c_z controls the rate of evolution and z_{max} is the maximum value that **z** can attain.

The fabric-dilatancy tensor was modified for the present model as,

$$dz = \frac{c_z}{1 + \langle \frac{z_{cum}}{2z_{max}} - 1 \rangle} \frac{\langle -d\varepsilon_v^{pl} \rangle}{D} (z_{max}\boldsymbol{n} + \boldsymbol{z}) \tag{2.57}$$

In this expression, the tensor **z** evolves in response to plastic deviatoric strains that occur during dilation only (i.e., dividing the plastic volumetric strain by the dilatancy gives plastic shear strain). In addition, the evolution of fabric is restricted to only occur when $(\boldsymbol{\alpha}^d - \boldsymbol{\alpha}) : \boldsymbol{n} < 0$; this additional constraint precludes fabric evolution during dilation above the rotated dilatancy surface (introduced later) but below the non-rotated

dilatancy surface. The parameter z_{cum} is the cumulative value of absolute changes in **z** computed according to,

$$dz_{cum} = |d\boldsymbol{z}| \tag{2.58}$$

The rate of evolution for **z** therefore decreases with increasing values of z_{cum}, which enables the undrained cyclic stress-strain response to progressively accumulate shear strains rather than lock-up into a repeating stress-strain loop. In addition, the greatest past peak value (scalar amplitude) for **z** during its loading history is also tracked,

$$z_{peak} = max\left(\sqrt{\frac{\boldsymbol{z}:\boldsymbol{z}}{2}}, z_{peak}\right) \tag{2.59}$$

The values of **z**, z_{peak}, and z_{cum} are later used to facilitate the accumulation of shear strains under symmetric loading through their effects on the plastic modulus and dilatancy relationships.

Additional memory of fabric formation history

Memory of the fabric formation history was included in the model presented herein to improve the ability of the model to account for the effects of sustained static shear stresses and account for differences in fabric effects for various drained versus undrained loading conditions.

The initial fabric tensor ($\boldsymbol{z}_{in}$) at the start of the current loading path is determined whenever a stress ratio reversal occurs, and thus correspond to the same times that the initial back-stress ratio and previous initial back-stress ratio are updated. The $\boldsymbol{z}_{in}$ tracks the immediate history terms without any consideration of whether an earlier loading cycle had produced greater degrees of fabric (i.e., the logic is different from that adopted for the updating of back-stress ratio history terms). This history term is used for describing the degree of stress rotation and its effects on plastic modulus, as described later.

Another aspect of the fabric history that is tracked is the mean stress at which the fabric is formed. This aspect of fabric history is tracked by tracking the product of **z** and p, and defining p_{zp} as the mean stress at the time that this product achieves its greatest peak value. The p_{zp} is used in addressing a couple of issues, including the issue of how fabric that is formed during liquefaction may be erased during reconsolidation. For example, saturated sand that develops cyclic mobility behavior during undrained cyclic loading clearly remembers its history of plastic deviatoric strains and then subsequently forgets (to a large extent) this prior strain history when it reconsolidates back to its pre-earthquake confining stress. As another example, the memory of prior strains during undrained cyclic loading is very different than the memory of prior strains during drained cyclic loading. This memory conceptually could be related to the history of plastic and total volumetric strains, but a simpler method to account 30 for this effect is to consider how the mean stress p relates to the value of p_{zp}. Conceptually, it appears that prior strain history (or fabric) is most strongly remembered when the soil is operating under mean stresses that are smaller than those that existed when the fabric was formed (i.e., $p << p_{zp}$) and then largely forgotten when they are of the same order (i.e., $p \approx p_{zp}$). This attribute will be used in the relationships described later for describing the effects of fabric on dilatancy.

Effect of fabric on plastic modulus

An effect of fabric on the plastic modulus was added to the model presented herein by reducing the plastic modulus as the fabric tensor increased in peak amplitude, as follows:

$$K_p = G \cdot h_o \cdot \frac{[(\boldsymbol{\alpha}^b - \boldsymbol{\alpha}):\boldsymbol{n}]^{0.5}}{\left[exp\left(\left(\boldsymbol{\alpha} - \boldsymbol{\alpha}_{in}^{app}\right):\boldsymbol{n}\right) - 1\right] + C_{\gamma 1}} C_{rev} \cdot \frac{C_{k\alpha}}{1 + C_{K_p}\left(\frac{z_{peak}}{z_{max}}\right)\langle(\boldsymbol{\alpha}^b - \boldsymbol{\alpha}):\boldsymbol{n}\rangle\sqrt{1 - C_{zpk2}}} \tag{2.60}$$

where,

$$C_{k\alpha} = 1 + \frac{C_{k\alpha f}}{1 + (2.5 \cdot \langle(\boldsymbol{\alpha} - \boldsymbol{\alpha}_{in}^{true}):\boldsymbol{n}\rangle)^2} \cdot C_{pzp2} \cdot C_{zpk1} \tag{2.61}$$

$$C_{zpk1} = \frac{z_{peak}}{z_{cum} + \frac{z_{max}}{5}} \tag{2.62}$$

$$C_{zpk2} = \frac{z_{peak}}{z_{cum} + \frac{z_{max}}{100}} \tag{2.63}$$

$$C_{pzp2} = \frac{-\langle-(p_{zp} - p)\rangle}{-\langle-(p_{zp} - p)\rangle + p_{min}} \tag{2.64}$$

The above expressions produce a reduction in plastic modulus when fabric is favorable (**z:n** ≥ 0) and with increasing plastic shear strains (which conceptually would break down any cementation). This reduces both the plastic modulus and the hysteretic damping at larger shear strains (note that z_{peak} = 0 unless the soil has been loaded strongly enough to pass outside the dilatancy surface), improves the volumetric strains that develop in drained cyclic loading, and improves the path in undrained cyclic loading.

The $C_{K\alpha}$ and square root of (1-C_{zpk2}) terms both serve to increase K_p during non-reversal loading by amounts that depend on the fabric and stress history. During reversal loading, the (1-C_{zpk2}) term approaches unity and K_p evolves as it previously had. The roles of each of the other terms are discussed below.

C_{zpk1} and C_{zpk2} are terms that start from zero and grow to be unity for uni-directional growth of fabric which is the case during non-reversing loading conditions. These two terms differ by the rate under which they approach unity by the use of the constant z_{max} /5 or z_{max} /100 with these respective values chosen for their ability to better approximate the engineering behaviors of interest and correlations that are shown later in the paper. For full reversal loading where the fabric alternates between positive and negative values, these terms will both go to zero.

C_{pzp2} starts initially at zero and stays equal to zero until fabric is formed. After fabric is formed, this term quickly transitions to unity for values of mean effective stress p that are less than the value that p had when the maximum fabric was formed (p_{zp}). If p increases beyond the value of p_{zp} the term will return to zero according to the MacCauley brackets.

The values for the calibration parameters C_{Kp} and $C_{K\alpha f}$ were chosen for their ability to reasonably approximate the targeted behaviors, as discussed later. Setting C_{Kp} to a default value of 2.0 was found to produce reasonable responses with particular emphasis on improving (reducing) the equivalent damping ratios at shear strains of 1 to 3% in drained cyclic loading. The parameter $C_{K\alpha f}$ is particularly useful for adjusting the undrained cyclic loading response with sustained static shear stresses; a default calibration which depends on D_R is presented later.

The cumulative effect of the above parameters can be understood as follows. If a soil is strongly loaded in uni-directional loading and forms significant amount of fabric and is then unloaded, then upon subsequent reloading the terms C_{pzp2} and C_{zpk1} will be unity and $C_{K\alpha}$ will become large. If the loads are increased to where the soil is being sheared and forming fabric at even higher stresses (higher values of p than fabric was previously formed at) then $C_{K\alpha}$ will be unity (C_{pzp2} = 0). In this way, an element that has developed

strong fabric under monotonic or cyclic loading without reversal of the total shear stress direction (e.g., an element within a steep slope where the static shear stresses are greater than the cyclic shear stresses) will, when unloaded and reloaded, be initially much stiffer (increased K_p) followed by a softening (smaller K_p) if the soil is loaded into virgin territory.

Effect of fabric on plastic volumetric dilation

A rotated dilatancy surface with slope M^{dR} which evolves with the history of the fabric tensor **z** was added to the framework of the model to facilitate earlier dilation at low stress ratios under certain loading paths (Ziotopoulou 2014). The rotated surface is equal to the original dilatancy surface scaled-down by a factor C_{rot1}:

$$M^{dR} = \frac{M^d}{C_{rot1}} \tag{2.65}$$

$$C_{rot1} = 1 + \frac{2 \cdot \langle -z:\boldsymbol{n} \rangle}{\sqrt{2} z_{max}} \cdot (1 - C_{zin1}) \geq 1 \tag{2.66}$$

where M^d is the slope of the unrotated dilatancy surface. Experimental results (Ziotopoulou 2014) indicate that the loading history, the loading direction and the loading pattern play important roles in the response of the soil to irregular cyclic loading. Thus the scaling factor that defines the rotated dilatancy surface was made dependent on whether fabric is favorable (**z : n** > 0) or unfavorable (**z : n** < 0) and on the factor C_{zin1} which is an indirect measure of whether there are reversals or not:

$$C_{zin1} = \langle 1 - exp\left(-2.0 \left| \frac{z_{in}:\boldsymbol{n} - z:\boldsymbol{n}}{z_{max}} \right| \right) \rangle \tag{2.67}$$

where $\mathbf{z_{in}}$ is the fabric tensor at the beginning of the current loading branch. C_{zin1} can take values ranging from 0, when there are no reversals, to 1, when there are reversals. The rotated dilatancy surface is operating only for loading with an unfavorable fabric since the factor C_{rot1} becomes 1 when the fabric is favorable (i.e., $\langle -\mathbf{z} : \mathbf{n} \rangle = 0$).

A back-stress ratio tensor for the rotated dilatancy surface (α^{dR}) was introduced as:

$$\alpha^{dR} = \frac{1}{\sqrt{2}} \cdot (M^{dR} - m)\boldsymbol{n} \tag{2.68}$$

Dilation occurs whenever the term ($\boldsymbol{\alpha}^{dR} - \boldsymbol{\alpha}$) : **n** is negative whereas contraction occurs when it is positive. The calculation of D is still treated separately during dilation and contraction.

D during dilation is now computed according to the following expressions. First, a value for D is computed from the rotated dilatancy surface:

$$D_{rot} = A_d \cdot \frac{\langle -z:\boldsymbol{n} \rangle}{\sqrt{2} z_{max}} \cdot \frac{(\alpha^{dR} - \alpha):\boldsymbol{n}}{C_{DR}} \tag{2.69}$$

where the C_{DR} factor is applied to reduce the rate under which dilatancy is increasing and is discussed further below. Second, another value for D is computed that would be obtained from the non-rotated dilatancy surface:

$$D_{non-rot} = A_d \cdot (-\langle -(\alpha^d - \alpha):\boldsymbol{n} \rangle) \tag{2.70}$$

The Macaulay brackets in the above expression ensure that $D_{non\text{-}rot}$ is equal to zero whenever ($\boldsymbol{\alpha}^{d} - \boldsymbol{\alpha}$) : **n** > 0 while ($\boldsymbol{\alpha}^{dR} - \boldsymbol{\alpha}$) : **n** < 0. Lastly, the operating value of D is selected from the above two values based on:

$$if\ \ D_{non-rot} < D_{rot} \Longrightarrow\ D = D_{non-rot}$$

$$else\ \ D = D_{non-rot} + (D_{rot} - D_{non-rot}) \cdot \frac{\langle M^{b} - M^{cur} \rangle}{\langle M^{b} - M^{cur} + 0.01 \rangle} \tag{2.71}$$

The above logic is illustrated in Figure 2.5 where D is plotted for a half cycle of loading that goes from contraction to dilation. This figure shows that $D_{non\text{-}rot}$ is used whenever it is smaller (more negative) than D_{rot}. For cases where D_{rot} is smaller than $D_{non\text{-}rot}$, the value of D is interpolated based on the additional term on the right that multiplies the difference between D_{rot} and $D_{non\text{-}rot}$. This interpolation term is close to unity for stress ratios away from the bounding surface ($M^{cur} < M^{b}$), such that D will be equal to D_{rot} as illustrated in the figure. However, this term will also go smoothly to zero as the stress ratio gets close to the bounding surface, so that dilatancy smoothly goes to zero as a soil approaches the critical state where $M = M^{d} = M^{b}$. The constant of 0.01 in the denominator controls the rate under which D goes to zero as the stress ratio nears the bounding surface and was found to provide reasonable results in trial simulations.

The factor C_{DR} in the denominator of the expression for D_{rot} is applied so that the D computed based on the rotated dilatancy surface is consistent with experimental observations. Its value, for the default calibration described later, has been made dependent on the initial D_R of the soil.

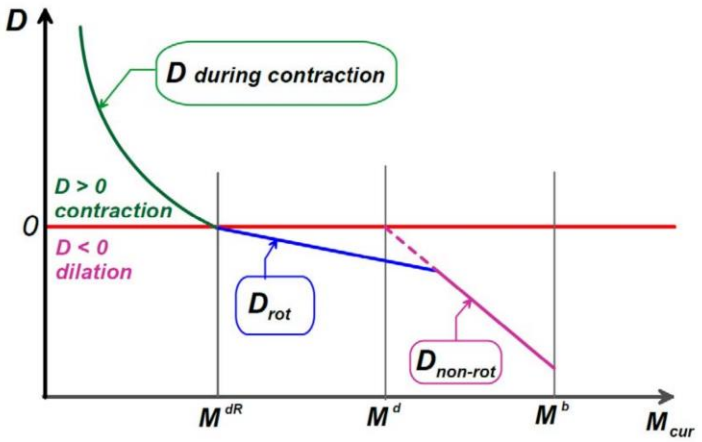

Figure 2.5. Schematic of the dilatancy D calculation based on the stress state with regards to the rotated dilatancy (M^{dR}), dilatancy (M^{d}) and bounding (M^{b}) surfaces during a half-cycle of loading that goes from contraction to dilation

Lastly, the parameter A_d in the expressions for both D_{rot} and $D_{non\text{-}rot}$ is expressed as,

$$A_d = \frac{A_{do}(C_{zin2})}{\left(\frac{z_{cum}}{z_{max}}^{2}\right)\left(1 - \frac{\langle -z : \boldsymbol{n} \rangle}{\sqrt{2} \cdot z_{peak}}\right)^{3} (C_{\varepsilon})^{2}(C_{pzp})(C_{pmin})(C_{zin1}) + 1} \tag{2.72}$$

$$C_{pzp} = \frac{1}{1 + \left(2.5p / p_{zp}\right)^{5}} \tag{2.73}$$

$$C_{pmin} = \frac{1}{1 + \left(p_{min2}/p\right)^2} \tag{2.74}$$

$$C_{zin1} = 1.0 - exp\left(-2.0\left|\frac{\boldsymbol{z}_{in}:\boldsymbol{n} - \boldsymbol{z}:\boldsymbol{n}}{z_{max}}\right|\right) \tag{2.75}$$

$$C_{zin2} = \frac{1 + C_{zin1}\dfrac{z_{cum} - z_{peak}}{3z_{max}}}{1 + 3 \cdot C_{zin1}\dfrac{z_{cum} - z_{peak}}{3z_{max}}} \tag{2.76}$$

Consider the six terms added to the denominator of the expression for A_d. The first term $[z_{cum}^2/z_{max}]$ facilitates the progressive growth of strains under symmetric loading by reducing the dilatancy that occurs when a liquefied soil has been sheared through many cycles of loading; note that this term progressively increases with subsequent cycles of loading. The second term facilitates strain-hardening when the plastic shear strain reaches the prior peak value, wherein the term approaches zero (i.e., when **z:n** approaches $z_{peak}\sqrt{2}$) and the dilation rate consequently rapidly approaches the virgin loading value of A_{do}. The third term C_ε is a calibration constant that can be used to modify the rate of plastic shear strain accumulation. The fourth term C_{pzp} causes the effects of fabric on dilation to be diminished (erased) whenever the current value of p is near the value of p_{zp}; this term enables the model to provide reasonable predictions of responses to large numbers of either drained or undrained loading cycles. The fifth term C_{pmin} provides a minimum amount of shear resistance for a soil after it has temporarily reached an excess pore pressure ratio of 100%; This term is almost zero when p'=0, such that the soil will initially dilate until some minimum p' has developed, after which the term quickly approaches 1.0. The parameter p_{min2} is currently set to become equal to 5% of the value of p' at consolidation (which is the value that exists when the flag FirstCall –see Section 3– was last set equal to 0), with the minimum value of p_{min2} being 10 times the minimum value of p' (i.e., p_{min} = 1/200 times the larger of p_A or the value of p' at consolidation). The sixth term C_{zin1} facilitates strain-hardening when stress reversals are not causing fabric changes; i.e., when the initial and current fabric terms are close to equal, the term C_{zin1} goes to zero. Lastly, the second term in the numerator, C_{zin2}, causes the dilatancy to be decreased by up to a factor of 3 under conditions of large strains and full stress (and fabric) reversals, which improves the prediction of cyclic strain accumulation during undrained cyclic loading.

An additional constraint is placed on D during dilation at very low effective stresses. For $p < 2p_{min}$, the value of D cannot be smaller in magnitude than computed by the following expression:

$$D = -3.5A_{do}\langle M^b - M^d\rangle\frac{2p_{min} - p}{p_{min}} \quad for \quad p_{min} \le p \le 2p_{min} \tag{2.77}$$

This expression ensures that the model will, for dense of critical soils (i.e., $M^b > M^d$), be dilative when p falls below $2p_{min}$.

Effect of fabric on plastic volumetric contraction

Dafalias and Manzari (2004) used the fabric tensor to modify the dilatancy during contraction (D > 0) as follows,

$$D = A_d \cdot [(\boldsymbol{\alpha}^d - \boldsymbol{\alpha}):\boldsymbol{n}](1 + \langle z:\boldsymbol{n}\rangle) \tag{2.78}$$

This relationship enhances the volumetric contraction whenever the fabric is favorable (**z:n** ≥ 0), based on the term 1+<z:n> as recommended by Dafalias and Manzari (2004).

The effect of fabric on dilatancy during contraction was modified for the present model as,

$$D = \mathrm{A}_{dc} \cdot \left[(\boldsymbol{\alpha} - \boldsymbol{\alpha}_{\boldsymbol{in}}^{\boldsymbol{app}}) : \boldsymbol{n} + C_{in} \right]^2 \frac{(\boldsymbol{\alpha}^d - \boldsymbol{\alpha}) : \boldsymbol{n}}{(\boldsymbol{\alpha}^d - \boldsymbol{\alpha}) : \boldsymbol{n} + C_D} C_{pmin2} \tag{2.79}$$

$$A_{dc} = \frac{\mathrm{A}_{do}(1 + \langle \boldsymbol{z} : \boldsymbol{n} \rangle)}{h_p C_{dz}} \tag{2.80}$$

$$C_D = 0.1 \tag{2.81}$$

$$C_{in} = \frac{2 \cdot \langle \boldsymbol{z} : \boldsymbol{n} \rangle}{\sqrt{2} z_{max}} \tag{2.82}$$

$$C_{dz} = \left(1 - C_{rot2} \cdot \frac{\sqrt{2} z_{peak}}{z_{max}}\right) \cdot \left(\frac{z_{max}}{z_{max} + C_{rot2} \cdot z_{cum}}\right) \geq \frac{1}{1 + \frac{z_{max}}{2}} \tag{2.83}$$

$$C_{rot2} = 1 - \frac{z_{peak}}{z_{cum} + \frac{z_{max}}{100}} \left(= 1 - C_{zpk2}\right) \tag{2.84}$$

$$\begin{aligned} C_{pmin2} &= 0 \quad for \quad p \leq 2p_{min} \\ C_{pmin2} &= 1 \quad for \quad p \geq 18p_{min} \\ C_{pmin2} &= \frac{p - 2p_{min}}{16p_{min}} \quad otherwise \end{aligned} \tag{2.85}$$

The factor C_{in} in the expression for D has been modified so it now depends on fabric; C_{in} is zero for unfavorable fabric, and increases with increasing **z:n** for favorable fabric to enhance the contraction rate at the start of an unloading cycle (note that D would be zero at the start of an unloading cycle if C_{in} was zero).

The term C_{dz} in the denominator of the expression for A_{dc} serves to increase the rate of contraction as z_{peak} nears z_{max} or as a large amount of cumulative fabric formation/destruction has taken place. This term was developed for improved modeling of the cyclic strength of denser sands, for which the value of h_p can be on the order of 100. The degrading of the denominator as z_{peak} or z_{cum} increases enables the generation of high excess pore pressures at higher loading levels, and controls the slope of the CRR versus number of uniform loading cycles relationship obtained for undrained element loading. Note that the denominator degrades whether fabric is favorable or not, but that the overall rate of contraction is more enhanced if the fabric is favorable (**z:n** ≥ 0). The factor C_{rot2} was introduced into the factor C_{dz} to provide better control over the rate of contraction as z_{peak} nears z_{max} or as a large amount of cumulative fabric formation/destruction has taken place. The factor C_{rot2} takes values that range from 1 for loading with zero fabric or cyclic loading that causes reversals of fabric (since z_{cum} will become much larger than z_{peak}), to 0 for loading that causes fabric to grow monotonically in one direction such as in non-reversal cyclic loading (since z_{cum} will equal z_{peak}). Lastly, the limit on the minimum value of C_{dz} is required for avoiding division by zero and to avoid over-estimating contraction rates (i.e., small values of h_p and large values of z_{peak} or z_{cum}).

The term C_{pmin2} slows the rate of contraction when p is approaching its minimum allowable value, and stops further contraction when p is less than twice the minimum allowable p.

Effect of fabric on the elastic modulus

The elastic shear modulus and elastic bulk modulus may degrade with increasing values of cumulative plastic deviator strain term, z_{cum}. This component of the model was added to account for the progressive destruction, with increasing plastic shear strains, of any minor cementation bonds or other ageing- or strain

history-related phenomena that produced an increase in small-strain shear modulus. The destruction of minor cementation by plastic shear strains is evidenced in the field by measurements of shear wave velocities in sand that are lower after earthquake shaking than before earthquake shaking (e.g., Arai 2006). The degradation of the elastic shear modulus is computed as,

$$G = G_o p_A \left(\frac{p}{p_A}\right)^{1/2} C_{SR} \left(\frac{1 + \frac{z_{cum}}{z_{max}}}{1 + \frac{z_{cum}}{z_{max}} C_{GD}}\right) \tag{2.86}$$

where C_{GD} is the factor by which the shear modulus is degraded (divided) at very large values of z_{cum}. This change in the elastic shear modulus G causes the bulk modulus K to progressively decrease with increasing z_{cum}. The change in K improves the model's ability to track the stress-strain response of liquefying sand. In particular, decreasing K with increasing z_{cum} reduces the rate of strain-hardening after phase transformation at larger shear strain levels, and improves the ability to approximate the hysteretic stress-strain response of a soil as it liquefies.

Effect of fabric on peak mobilized friction angles in drained and undrained loading

Kutter and Chen (1997) showed that plastic dilation rates are different in drained and undrained loading of the same clean sand, with the consequence being that the peak mobilized friction angles are also different for drained and undrained loading. This aspect of behavior would appear to be contradictory to having a bounding surface that is only dependent on the relative state of the sand (i.e., through the parameter n^b) if the mobilized friction angles for drained and undrained loading paths are both controlled by the bounding surface. The model presented herein produces the same peak mobilized friction angles for drained and undrained loading because both conditions become limited by the same bounding surface. This aspect of behavior deserves closer examination in future efforts.

2.9- Post-shaking reconsolidation

Volumetric strains that develop during post-liquefaction reconsolidation of sand are difficult to numerically model using the conventional constitutive separation of strains into elastic and plastic components since a large portion of the post-liquefaction reconsolidation strains are due to sedimentation effects which are not easily incorporated into either the elastic or plastic components of behavior. Single element simulations using various constitutive models show that they generally predict post-liquefaction reconsolidation strains that are an order of magnitude smaller than observed in various experimental studies (e.g., Ziotopoulou and Boulanger 2013b, Howell et al. 2014).

The present model was modified to provide more realistic estimates of reconsolidation strains during the post-shaking portion of a numerical simulation. The modification involved the pragmatic approach of reducing the post-shaking elastic shear modulus G (and hence elastic bulk modulus K) which increases reconsolidation strains, thereby compensating for the sedimentation strains which are not explicitly modeled. The user may activate this feature after the end of strong shaking, such that post-liquefaction reconsolidation strains are better approximated in the remainder of the simulation. This feature should not be activated for the strong shaking portion of a simulation.

The post-shaking elastic moduli are determined by multiplying the conventional elastic moduli (computed using the expressions described earlier) by a reduction factor F_{sed} as,

$$G_{post-shaking} = F_{sed} G \tag{2.87}$$

$$K_{post-shaking} = F_{sed} K \tag{2.88}$$

The F_{sed} value is computed as,

$$F_{sed} = F_{sed,min} + \left(1 - F_{sed,min}\right)\left(\frac{p'}{20p'_{sed}}\right) \leq 1 \tag{2.89}$$

$$p'_{sed} = p'_{sed_o}\left(\frac{z_{cum}}{z_{cum} + z_{max}}\right)\langle 1 - \frac{M^{cur}}{M^d}\rangle^{0.25} \tag{2.90}$$

$$F_{sed,min} = 0.03 \cdot exp(2.6 \cdot D_R) \leq 0.99 \tag{2.91}$$

$$p'_{sed_o} = -\frac{P_{atm}}{5} \tag{2.92}$$

where the constant value $F_{sed,min}$ represents the smallest value that F_{sed} can attain and is dependent on the initial relative density, and the parameter $p'_{sed,o}$ is the mean effective stress up to which reconsolidation strains are enhanced. The value of F_{sed} progressively reduces from unity toward the value of $F_{sed,min}$ as z_{cum} progressively increases and provided that M^{cur} is less than M^d . Setting $F_{sed,min} = 0.04$ was found to produce reasonable responses as shown later. The user can select values for $p'_{sed,o}$ and $F_{sed,min}$.

2.10- Summary of constitutive equations

The constitutive equations for the model presented herein are summarized in Table 2.1 along with the equations for the Dafalias-Manzari (2004) model.

Dafalias-Manzari (2004) model	***Present model***
Critical state line $e_{cs} = e_o - \lambda\left(\frac{p_{cs}}{p_A}\right)^{\xi}$	***Critical state line*** $\xi_R = \frac{R}{Q - \ln\left(100\frac{p}{p_A}\right)} - D_R$
Elastic deviatoric strain increment $d\boldsymbol{e}^{el} = \frac{d\mathbf{s}}{2G}$ $G = G_o p_A \frac{(2.97-e)^2}{1+e}\left(\frac{p}{p_A}\right)^{1/2}$	***Elastic deviatoric strain increment*** $d\boldsymbol{e}^{el} = \frac{d\mathbf{s}}{2G}$ $G = G_o p_A \left(\frac{p}{p_A}\right)^{1/2} C_{SR}\left(\frac{1+\frac{z_{cum}}{z_{max}}}{1+\frac{z_{cum}}{z_{max}}C_{GD}}\right)$ $C_{SR} = 1 - C_{SR,o} \cdot \left(\frac{M}{M^b}\right)^{m_{SR}}$ $C_{SR,o} = 0.5$ $m_{SR} = 4$
Elastic volumetric strain increment $d\varepsilon_v^{el} = \frac{dp}{K}$	***Elastic volumetric strain increment*** $d\varepsilon_v^{el} = \frac{dp}{K}$

$K = \frac{2(1+v)}{3(1-2v)} G$	$K = \frac{2(1+v)}{3(1-2v)} G$
Yield surface $f = [(\boldsymbol{s} - p\boldsymbol{\alpha}) : (\boldsymbol{s} - p\boldsymbol{\alpha})]^{1/2} - \sqrt{2/3} pm = 0$	***Yield surface*** $f = [(\boldsymbol{s} - p\boldsymbol{\alpha}) : (\boldsymbol{s} - p\boldsymbol{\alpha})]^{1/2} - \sqrt{1/2} pm = 0$
Plastic deviatoric strain increment $d\boldsymbol{e}^{pl} = \langle L \rangle \boldsymbol{R}'$ $\boldsymbol{R} = B\boldsymbol{n} - C\left(\boldsymbol{n}^2 - \frac{1}{3}\boldsymbol{I}\right) + \frac{1}{3} D\boldsymbol{I}$ $B = 1 + \frac{3}{2}\frac{1-c}{c} g(\theta, c)\cos(\theta)$ $C = 3\sqrt{\frac{3}{2}}\frac{1-c}{c} g(\theta, c)$ $c = \frac{Q_{ext}}{Q_{compr}}$ $g(\theta, c) = \frac{2c}{(1+c)-(1-c)\cos(3\theta)}$ $M^b = M \cdot exp\left(-n^b \xi_R\right)$ $\boldsymbol{\alpha}_\theta^b = \sqrt{2/3}\,[g(\theta, c) M^b - m]\boldsymbol{n}$ $K_p = \frac{2}{3} G \cdot h_o \cdot \frac{\left(\boldsymbol{\alpha}_\theta^b - \boldsymbol{\alpha}\right) : \boldsymbol{n}}{(\boldsymbol{\alpha} - \boldsymbol{\alpha}_{in}) : \boldsymbol{n}}$	***Plastic deviatoric strain increment*** $d\boldsymbol{e}^{pl} = \langle L \rangle \boldsymbol{R}'$ $\boldsymbol{R} = \boldsymbol{R}' + \frac{1}{3} D\boldsymbol{I} = \boldsymbol{n} + \frac{1}{3} D\boldsymbol{I}$ $M^b = M \cdot exp\left(-n^b \xi_R\right)$ $M = 2 \cdot \sin\left(\phi_{cv}\right)$ $\boldsymbol{\alpha}^b = \sqrt{1/2}\,[M^b - m]\boldsymbol{n}$ $K_p = G \cdot h_o \cdot \frac{[(\boldsymbol{\alpha}^b - \boldsymbol{\alpha}) : \boldsymbol{n}]^{0.5}}{\left[exp\left((\boldsymbol{\alpha} - \boldsymbol{\alpha}_{in}^{app}) : \boldsymbol{n}\right) - 1\right] + C_{\gamma 1}} C_{rev} \cdot \frac{C_{k\alpha}}{1 + C_{Kp}\left(\frac{z_{peak}}{z_{max}}\right)\langle(\boldsymbol{\alpha}^b - \boldsymbol{\alpha}) : \boldsymbol{n}\rangle\sqrt{1 - C_{zpk2}}}$ $C_{rev} = \frac{(\boldsymbol{\alpha} - \boldsymbol{\alpha}_{in}^{app}) : \boldsymbol{n}}{(\boldsymbol{\alpha} - \boldsymbol{\alpha}_{in}^{true}) : \boldsymbol{n}} \;\; for \;\; \left(\boldsymbol{\alpha} - \boldsymbol{\alpha}_{in}^{p}\right) : \boldsymbol{n} \leq \boldsymbol{0}$ $= 1 \; otherwise$ $C_{k\alpha} = 1 + \frac{C_{k\alpha f}}{1 + \left(2.5 \cdot \langle(\boldsymbol{\alpha} - \boldsymbol{\alpha}_{in}^{true}) : \boldsymbol{n}\rangle\right)^2} \cdot C_{pzp2} \cdot C_{zpk1}$ $C_{zpk1} = \frac{z_{peak}}{z_{cum} + \frac{z_{max}}{5}}$ $C_{zpk2} = \frac{z_{peak}}{z_{cum} + \frac{z_{max}}{100}}$ $C_{pzp2} = \frac{-\langle -(p_{zp} - p)\rangle}{-\langle -(p_{zp} - p)\rangle + p_{min}}$ $C_{\gamma 1} = \frac{h_o}{200}$ $C_{Kp} = 2$
Plastic volumetric strain increment $d\varepsilon_v^{pl} = \langle L \rangle D$ $M^d = M \cdot exp\left(n^d \xi_R\right)$ $\boldsymbol{\alpha}_\theta^d = \sqrt{2/3}\,[g(\theta, c) M^d - m]\boldsymbol{n}$ $D = A_{do} \cdot \left[\left(\boldsymbol{\alpha}_\theta^d - \boldsymbol{\alpha}\right) : \boldsymbol{n}\right]$	***Plastic volumetric strain increment***

$A_d = \mathrm{A}_o(1 + \langle \boldsymbol{z}{:}\,\boldsymbol{n} \rangle)$	$d\varepsilon_v^{pl} = \langle L \rangle D$ $M^d = M \cdot exp\left(n^d \xi_R\right)$ $M^{dR} = \frac{M^d}{C_{rot1}}$ $C_{rot1} = 1 + \frac{2 \cdot \langle -z:\boldsymbol{n} \rangle}{\sqrt{2} z_{max}} \cdot (1 - C_{zin1}) \geq 1$ $C_{zin1} = \langle 1 - exp\left(-2.0 \left\lvert \frac{z_{in}:\boldsymbol{n} - z:\boldsymbol{n}}{z_{max}} \right\rvert\right) \rangle$ $\alpha^d = \frac{1}{\sqrt{2}} \cdot (M^d - m)\boldsymbol{n}$ $\alpha^{dR} = \frac{1}{\sqrt{2}} \cdot (M^{dR} - m)\boldsymbol{n}$ $If\ dilating\ (D < 0)$: $D_{non-rot} = A_d \cdot [(\boldsymbol{\alpha}^d - \boldsymbol{\alpha}){:}\,\boldsymbol{n}]$ $D_{rot} = A_d \cdot \frac{\langle -z:\boldsymbol{n} \rangle}{\sqrt{2} z_{max}} \cdot \frac{(\alpha^{dR} - \alpha):\boldsymbol{n}}{C_{DR}}$ $if\ \ D_{non-rot} < D_{rot} \Longrightarrow\ D = D_{non-rot}$ $else\ \ D = D_{non-rot} + (D_{rot} - D_{non-rot}) \cdot \frac{\langle M^b - M^{cur} \rangle}{\langle M^b - M^{cur} + 0.01 \rangle}$ $A_d = \frac{A_{do}(C_{zin2})}{\left(\frac{z_{cum}{}^2}{z_{max}}\right)\left(1 - \frac{\langle -z:\boldsymbol{n} \rangle}{\sqrt{2} \cdot z_{peak}}\right)^3 (C_\varepsilon)^2 (C_{pzp})(C_{pmin})(C_{zin1}) + 1}$ $A_{do} = \frac{1}{0.4} \cdot \frac{\left[\sin^{-1}\left(\frac{M^b}{2}\right) - \sin^{-1}\left(\frac{M}{2}\right)\right]}{M^b - M^d}$ $C_{pzp} = \frac{1}{1 + \left(2.5p / p_{zp}\right)^5}$ $C_{pmin} = \frac{1}{1 + \left(p_{min2} / p\right)^2}$ $C_{zin1} = 1.0 - exp\left(-2.0 \left\lvert \frac{\boldsymbol{z_{in}}:\boldsymbol{n} - \boldsymbol{z}:\boldsymbol{n}}{z_{max}} \right\rvert\right)$ $C_{zin2} = \frac{1 + C_{zin1} \frac{z_{cum} - z_{peak}}{3 z_{max}}}{1 + 3 \cdot C_{zin1} \frac{z_{cum} - z_{peak}}{3 z_{max}}}$ $If\ contracting\ (D \geq 0)$ $D = \mathrm{A}_{dc} \cdot \left[(\boldsymbol{\alpha} - \boldsymbol{\alpha_{in}^{app}}){:}\,\boldsymbol{n} + C_{in}\right]^2 \frac{(\boldsymbol{\alpha}^d - \boldsymbol{\alpha}):\boldsymbol{n}}{(\boldsymbol{\alpha}^d - \boldsymbol{\alpha}):\boldsymbol{n} + C_D} \leq 1.5 \cdot A_{do} \frac{(\boldsymbol{\alpha}^d - \boldsymbol{\alpha}):\boldsymbol{n}}{(\boldsymbol{\alpha}^d - \boldsymbol{\alpha}):\boldsymbol{n} + C_D}$ $A_{dc} = \frac{\mathrm{A}_{do}(1 + \langle \boldsymbol{z}:\boldsymbol{n} \rangle)}{h_p C_{dz}}$

	$C_{in} = \frac{2\langle \boldsymbol{z}:\boldsymbol{n}\rangle}{\sqrt{2}z_{max}}$ $C_{dz} = \left(1 - C_{rot2} \cdot \frac{\sqrt{2}z_{peak}}{z_{max}}\right) \cdot \left(\frac{z_{max}}{z_{max}+C_{rot2}z_{cum}}\right) \geq \frac{1}{1+\frac{z_{max}}{2}}$ $C_{rot2} = 1 - \frac{z_{peak}}{z_{cum}+\frac{z_{max}}{100}} \left(= 1 - C_{zpk2}\right)$ $C_D = 0.1$ $h_p = h_{po}\ exp\left(-0.7 + 7.0\left(0.5 - \xi_R\right)^2\right)\ for\ \xi_R \leq 0.5$ $h_p = h_{po}\ exp(-0.7)\ \ for\ \xi_R > 0.5$
Fabric-dilatancy tensor update $dz = -c_z\langle -d\varepsilon_v^{pl}\rangle(z_{max}\boldsymbol{n} + \boldsymbol{z})$	***Fabric-dilatancy tensor update if*** **($\alpha^d - \alpha$):n** < 0 $dz = \frac{c_z}{1+\langle\frac{z_{cum}}{2z_{max}}-1\rangle}\frac{\langle -d\varepsilon_v^{pl}\rangle}{D}(z_{max}\boldsymbol{n} + \boldsymbol{z})$ $dz_{cum} = \lvert d\boldsymbol{z}\rvert$
Stress increment $L = \frac{2G\boldsymbol{n}:d\boldsymbol{e} - \boldsymbol{n}:\boldsymbol{r}Kd\varepsilon_v}{K_p + 2G\left(B - C\cdot tr\boldsymbol{n}^3\right) - KD\boldsymbol{n}:\boldsymbol{r}}$ $d\boldsymbol{\sigma} = 2Gd\boldsymbol{e} + Kd\varepsilon_v\boldsymbol{I} - \langle L\rangle\left(2G\left[B\boldsymbol{n}\left(\boldsymbol{n}^2 - \frac{1}{3}\right)\boldsymbol{I}\right] + KD\boldsymbol{I}\right)$	***Stress increment*** $L = \frac{2G\boldsymbol{n}:d\boldsymbol{e} - \boldsymbol{n}:\boldsymbol{r}Kd\varepsilon_v}{K_p + 2G - KD\boldsymbol{n}:\boldsymbol{r}}$ $d\boldsymbol{\sigma} = 2Gd\boldsymbol{e} + Kd\varepsilon_v\boldsymbol{I} - \langle L\rangle(2G\boldsymbol{n} + KD\boldsymbol{I})$
	Post-shaking reconsolidation $G_{post-shaking} = F_{sed}G$ $K_{post-shaking} = F_{sed}K$ $F_{sed} = F_{sed,min} + \left(1 - F_{sed,min}\right)\left(\frac{p'}{20p'_{sed}}\right) \leq 1$ $p'_{sed} = p'_{sed_o}\left(\frac{z_{cum}}{z_{cum}+z_{max}}\right)\langle 1 - \frac{M^{cur}}{M^d}\rangle^{0.25}$ $F_{sed,min} = 0.03 \cdot exp(2.6 \cdot D_R) \leq 0.99$ $p'_{sed_o} = -\frac{P_{atm}}{5}$

Table 2.1. Comparison of constitutive equations

3- Examples and Verifications

The PM4Sand primary model parameters consists of three main properties, the atmospheric pressure and two flags. The rest of model parameters have default values that automatically can be assigned to or calculated for them. In RS2 the later set of parameters have their default values in their dialog field or have "Auto Calculate" option. The users have the option of choosing the default values for these variables or change them as they would see fit.

The three primary input properties are the relative density (D_R) of sand, the shear modulus coefficient (G_o), and the contraction rate parameter (h_{po}).

For the purpose of verification series of simulations are considered that include Drained Direct Simple Shear Test, Undrained Direct Simple Shear Test and Undrained Cyclic Direct Simple Shear Tests. The primary parameters of the loos, medium dense and dense sands are presented in table 3.1. The RS2 results are compared mainly with the results from FLAC and PLAXIS. The FLAC results are obtained using the constitutive model dll file and FLAC model and FISH files from the original work by Boulanger, R. W., and Ziotopoulou, K. (https://pm4sand.engr.ucdavis.edu/pm4sand-files).

D_R	G_o	h_{po}
0.35	476	0.53
0.55	677	0.40
0.75	890	0.63

Table 3.1. Input parameters for PM4Sand model verifications

3.1- Drained Monotonic Direct Simple Shear Tests

The response for drained monotonic direct simple shear tests (DSS plane-strain) for sand at D_R of 35%, 55%, and 75% with properties listed in Table 3.1, under vertical confining stresses of 0.25, 1, 4, and 16 atmospheric pressure are presented shown in Figures 3.1 to 3.5.

All the simulations are done under strain control loading and there is a good agreement between the results generated by the three software.

3.2- Undrained Monotonic Direct Simple Shear Tests

The response for undrained monotonic direct simple shear tests (DSS plane-strain) for sand at D_R of 35%, 55%, and 75% with properties listed in Table 3.1, under vertical confining stresses of 0.25, 1, 4, and 16 atmospheric pressure are presented shown in Figures 3.6 to 3.10.

All the simulations are done under strain control loading and there is a good agreement between the results generated by the three software.

3.3- Undrained Cyclic Direct Simple Shear Tests

The response for undrained cyclic direct simple shear tests (DSS plane-strain) for sand at D_R of 35%, 55%, and 75% with properties listed in Table 3.1, under vertical confining stress of 1atmospheric pressure are presented shown in Figures 3.11 to 3.16. for each relative density of sand 2 different levels of maximum shear stress to initial effective vertical stress is considered. The simulations in FLAC are strain controlled and the loading direction changes when the shear stress reaches to the maximum/minimum values. Since the strains increments are small the maximum and minimum values of shear stress match the assigned values with an acceptable accuracy. This minor error could accumulate when the number of cycles increase, and the results might deviate form an ideal stress path with fixed minimum and maximum shear stresses. The loading in RS2 and PLAXIS is stress controlled and the accuracy of the maximum and minimum shear stresses are controlled by the tolerance defined for the convergence of the solution in these tools. Due to the difference in the loading, being strain or stress controlled, and the acceptable tolerance for the convergency of solution there are minor differences between the results. This is more pronounced in Figures 3.11 and 3.12 where the stress path predicted by FLAC shows a decrease in shear stress with increasing shear strain. Both RS2 and PLAXIS in this case do not show the decrease in the shear stress, as the simulations are stress controlled, but they show a big jump in the value of shear strain. Other than this difference that is expected there is a good agreement between the results generated by the three software.

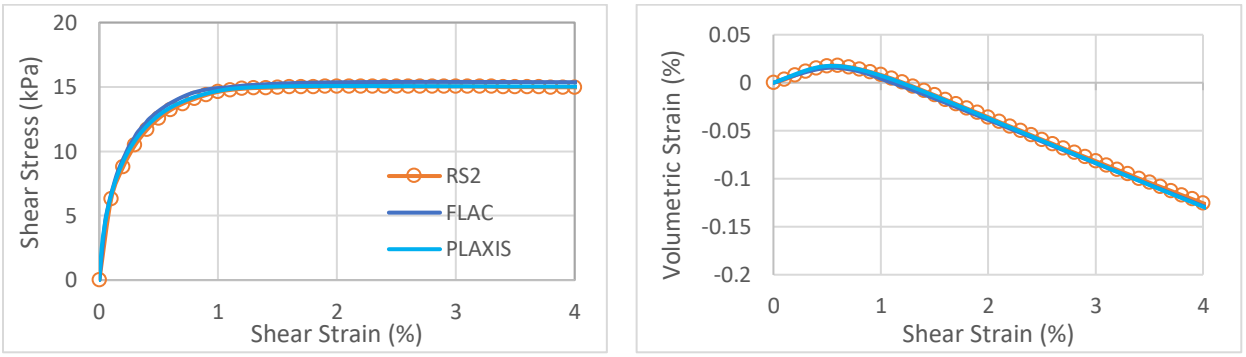

(a)

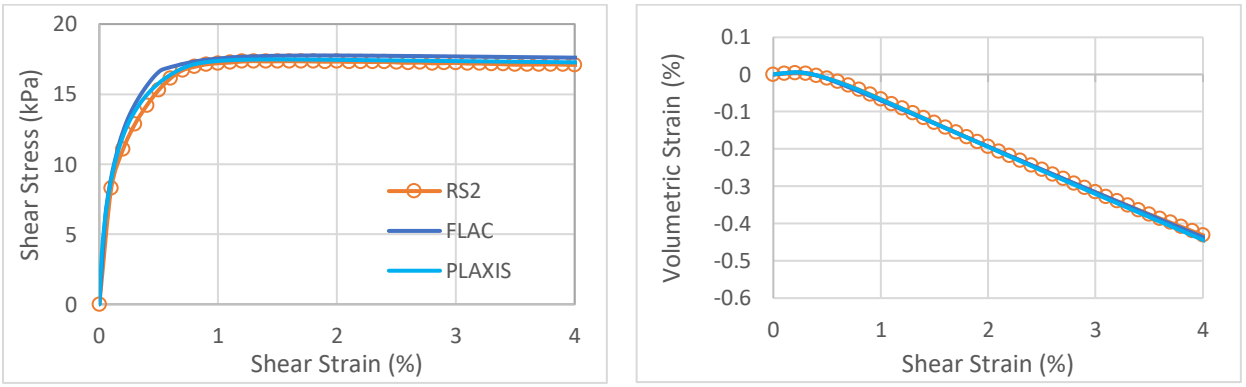

(b)

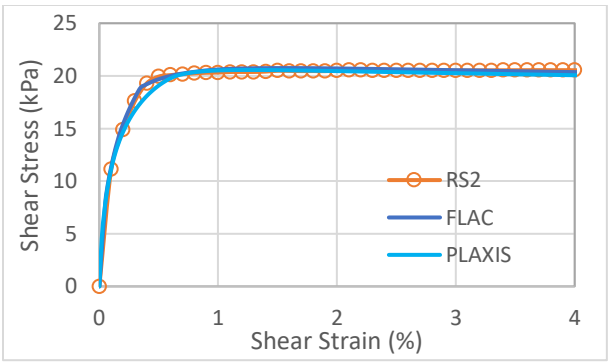

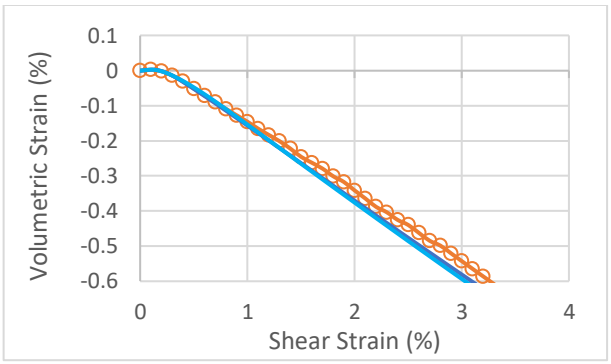

(c)

Figure 3.1. Monotonic Drained Simple Shear Test loading responses for (a) D_R = 35% (b) D_R =55, and (c) D_R=75% with vertical effective stress of ¼ P_{atm}, and Ko=0.5

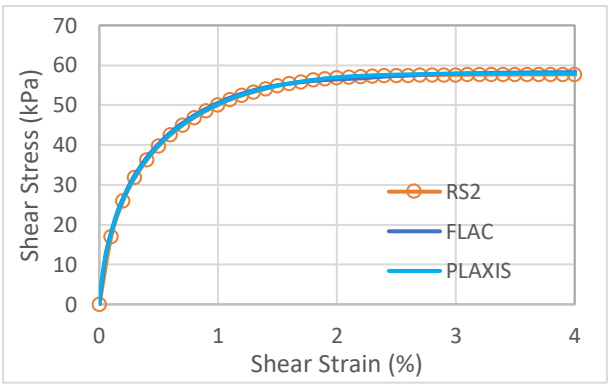

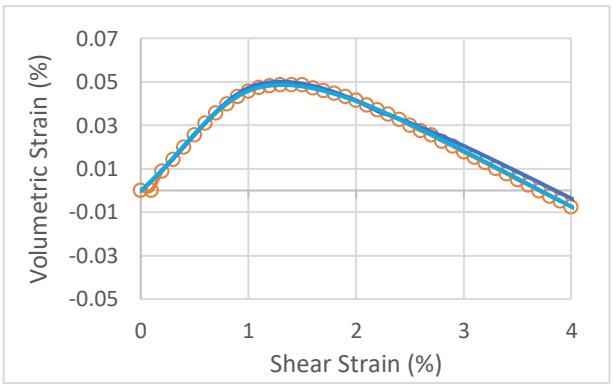

(a)

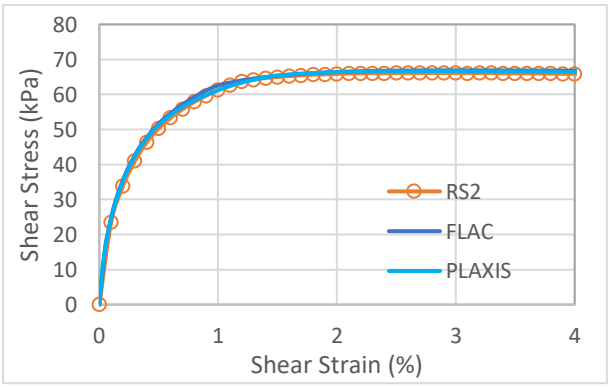

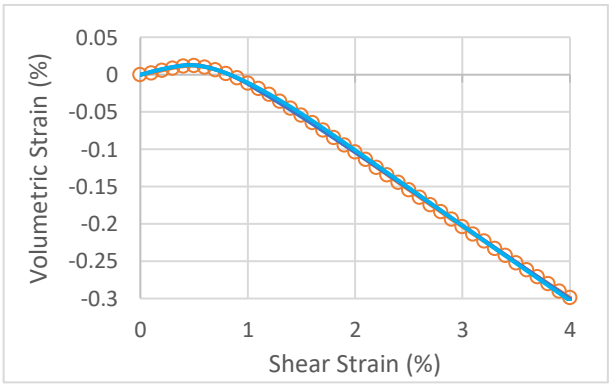

(b)

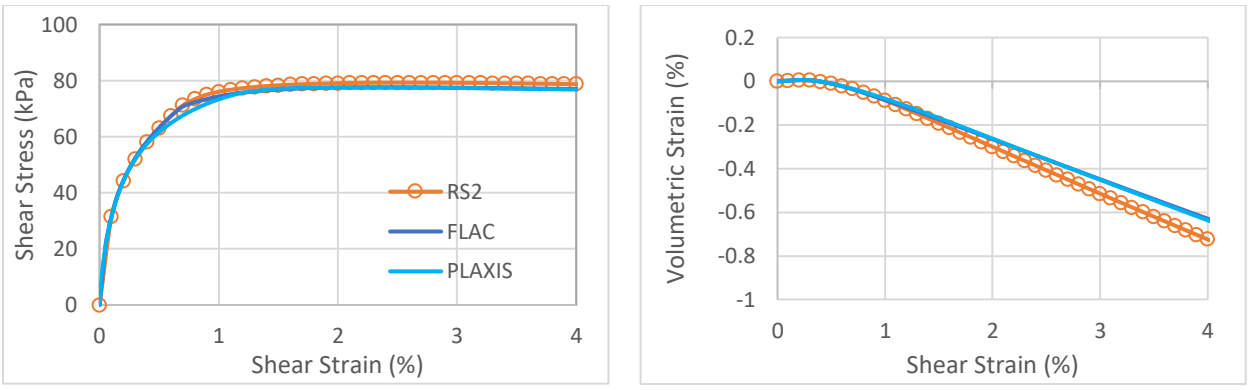

(c)

Figure 3.2. Monotonic Drained Simple Shear Test loading responses for (a) D_R = 35% (b) D_R =55, and (c) D_R=75% with vertical effective stress of 1 P_{atm}, and Ko=0.5

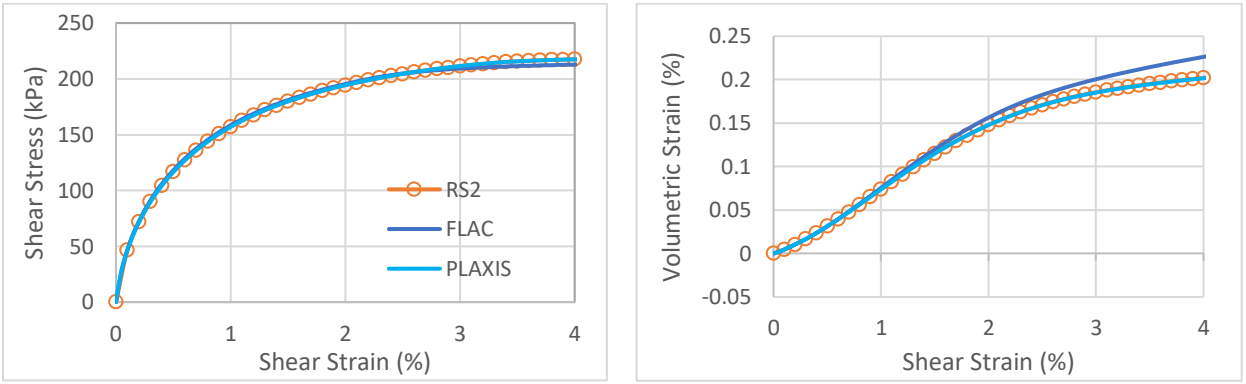

(a)

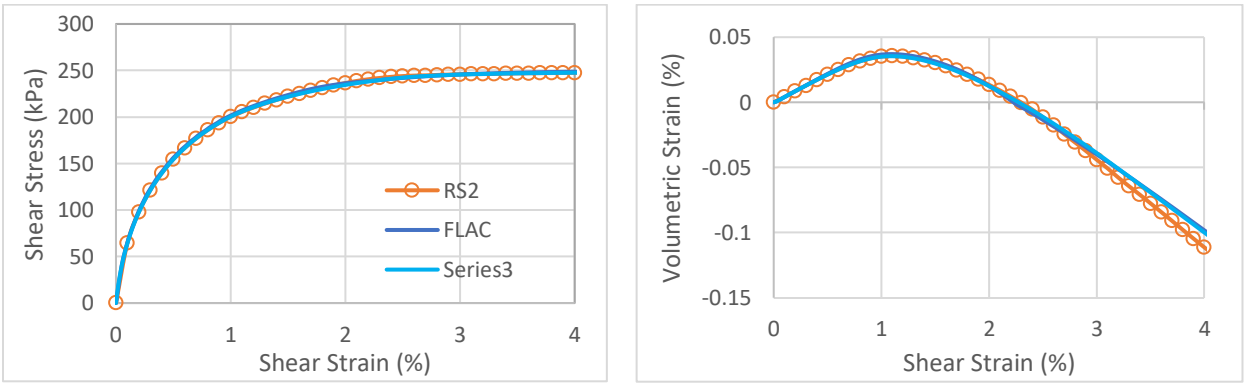

(b)

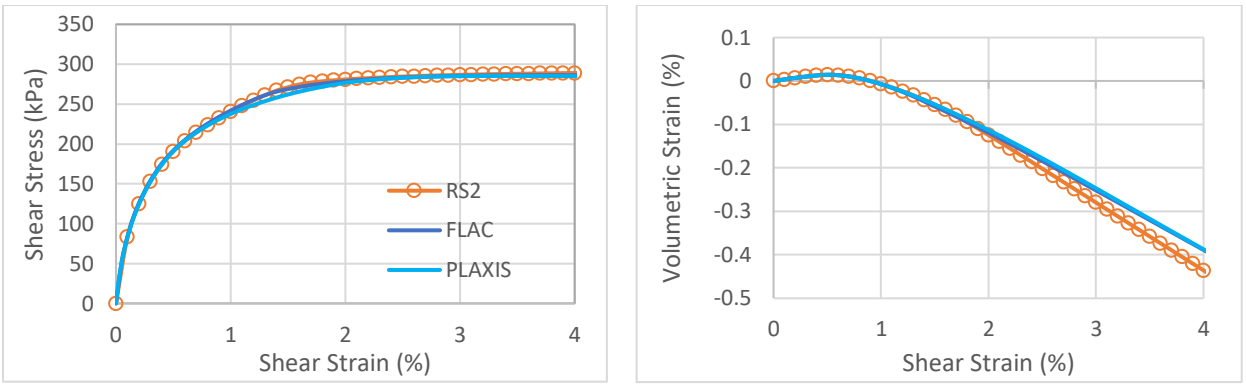

(c)

Figure 3.3. Monotonic Drained Simple Shear Test loading responses for (a) D_R = 35% (b) D_R =55, and (c) D_R=75% with vertical effective stress of 4 P_{atm}, and Ko=0.5

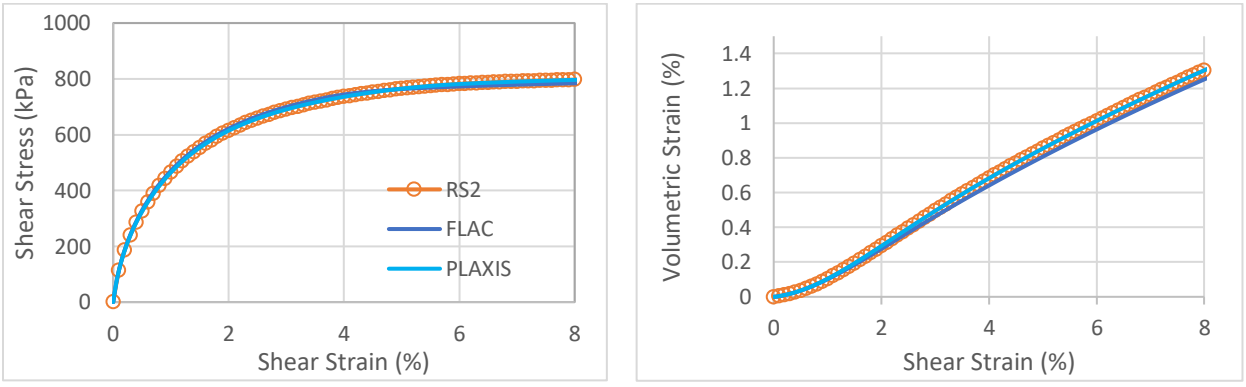

(a)

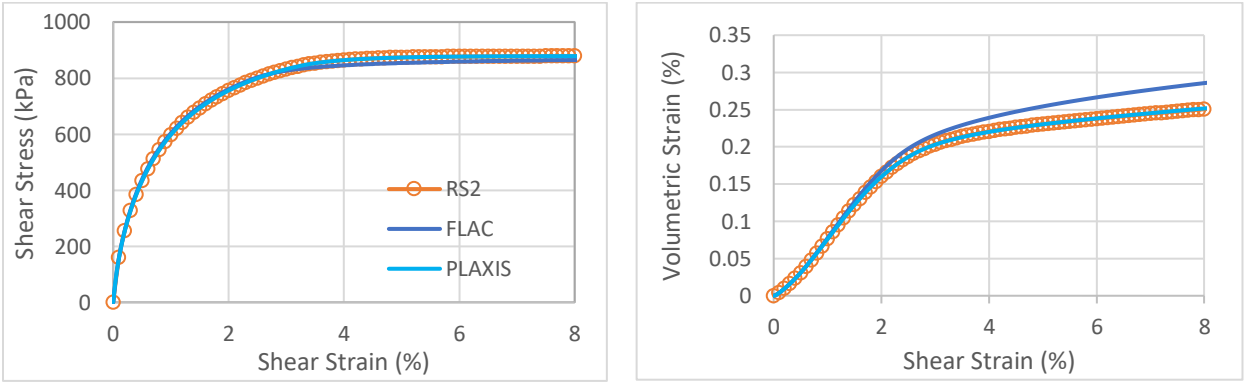

(b)

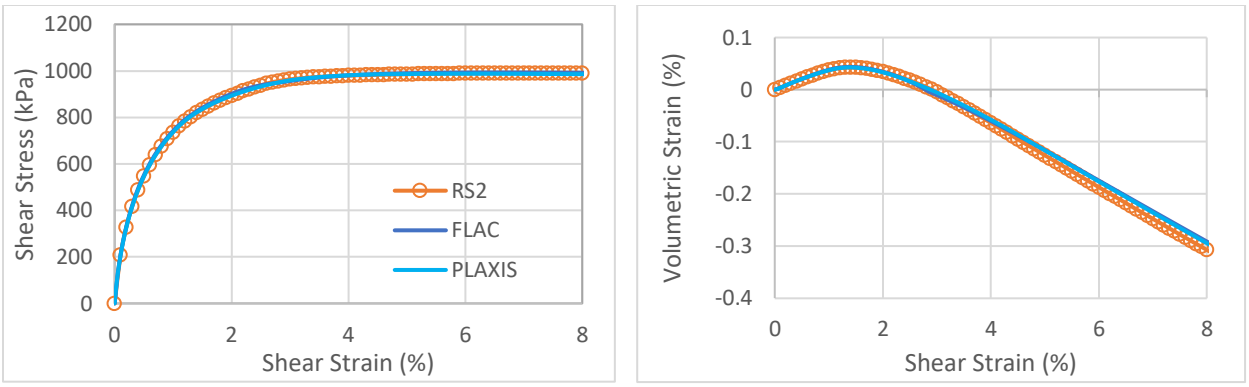

(c)

Figure 3.4. Monotonic Drained Simple Shear Test loading responses for (a) D_R = 35% (b) D_R =55, and (c) D_R=75% with vertical effective stress of 16 P_{atm}, and Ko=0.5

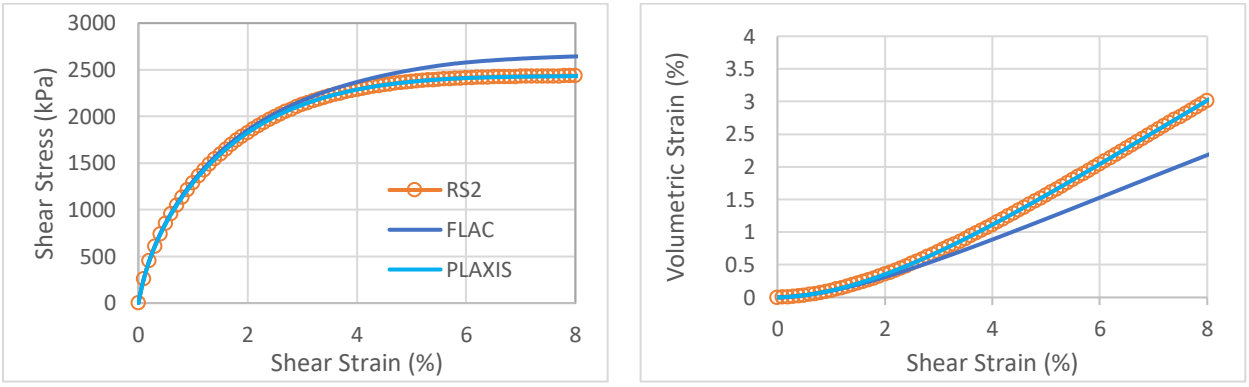

(a)

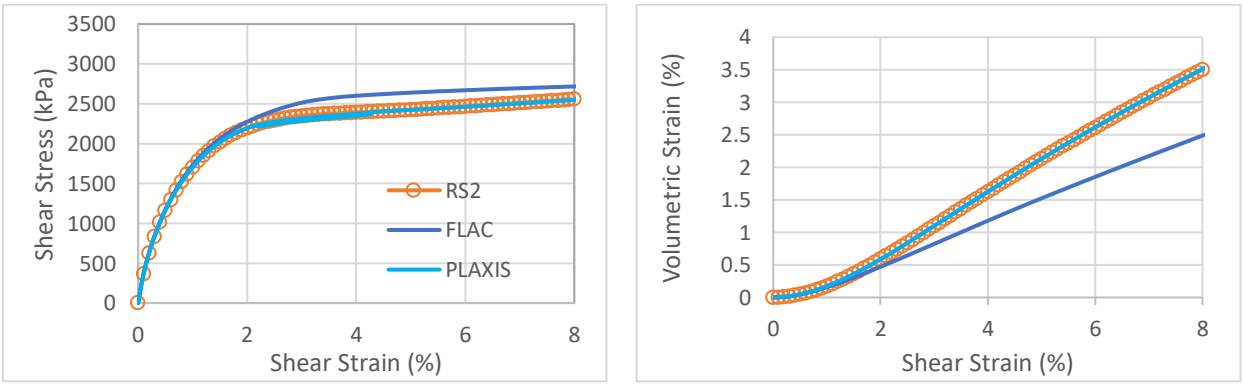

(b)

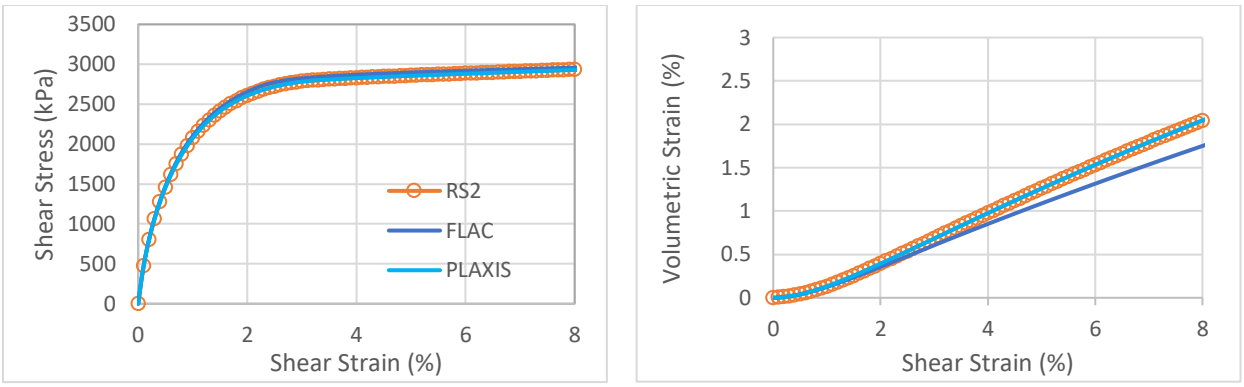

(c)

Figure 3.5. Monotonic Drained Simple Shear Test loading responses for (a) D_R = 35% (b) D_R =55, and (c) D_R=75% with vertical effective stress of 64 P_{atm}, and Ko=0.5

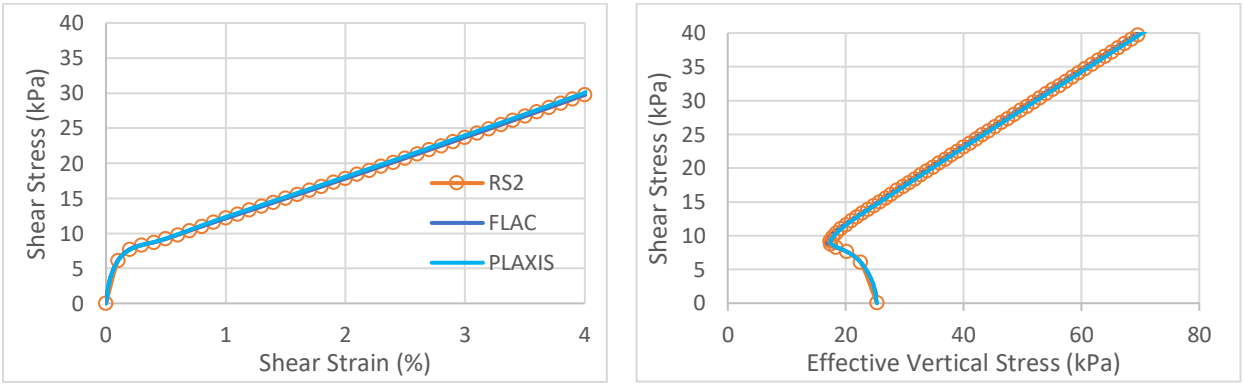

(a)

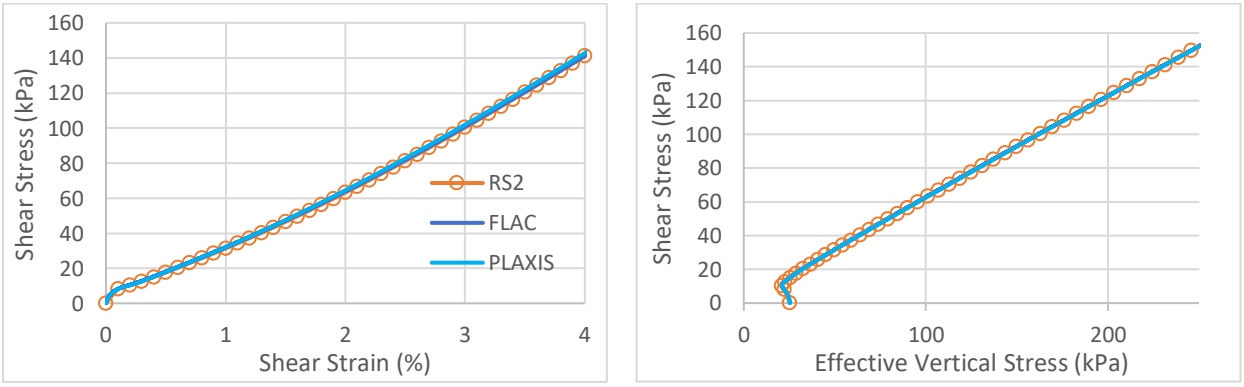

(b)

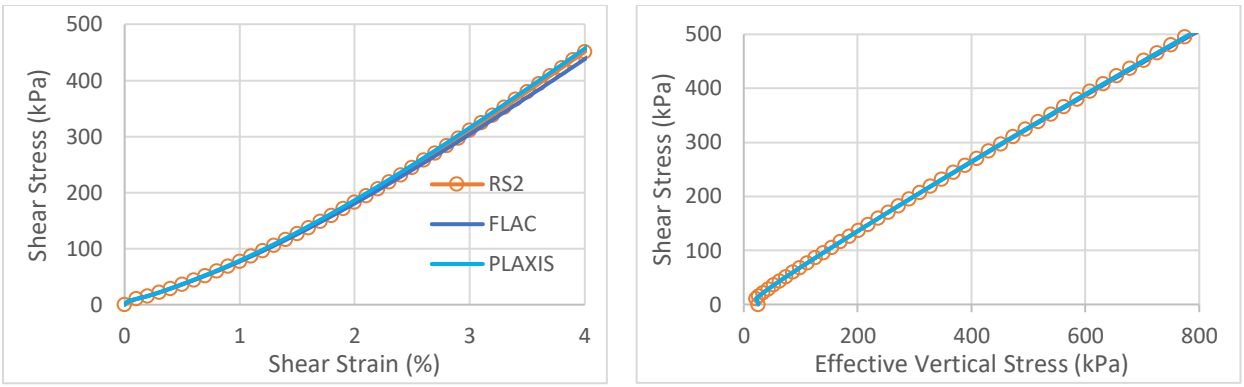

(c)

Figure 3.6. Monotonic Undrained Simple Shear Test loading responses for (a) D_R = 35% (b) D_R =55, and (c) D_R=75% with vertical effective stress of ¼P_{atm}, and Ko=0.5

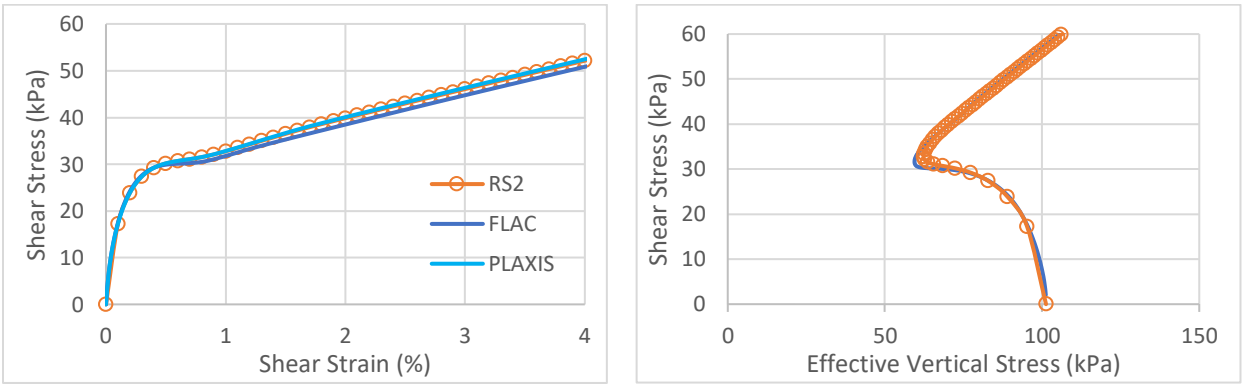

(a)

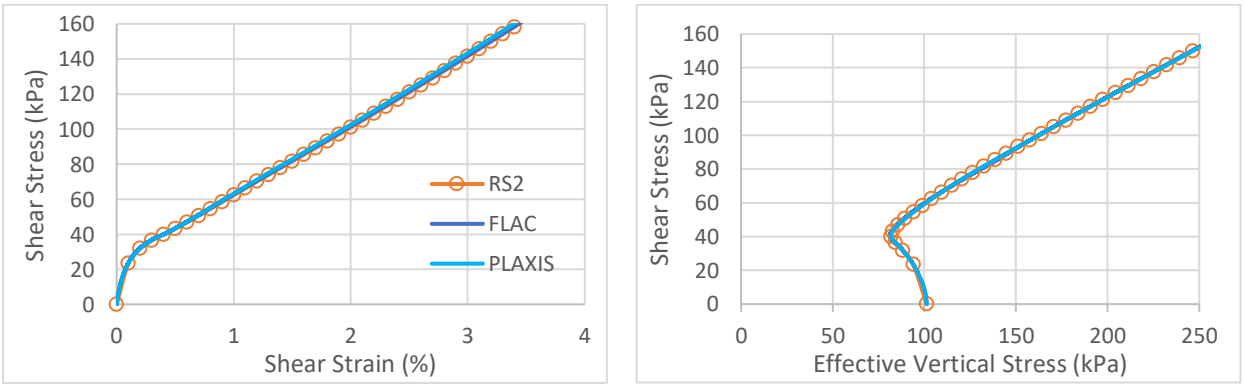

(b)

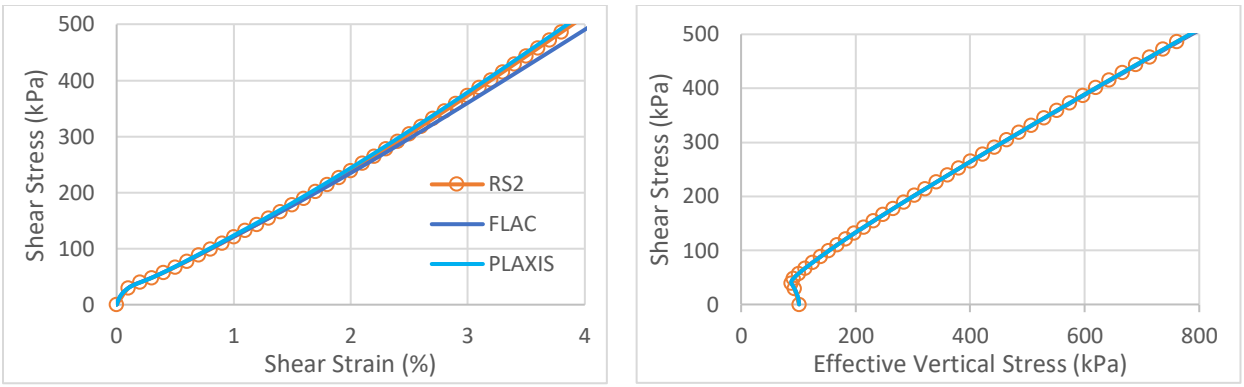

(c)

Figure 3.7. Monotonic Undrained Simple Shear Test loading responses for (a) D_R = 35% (b) D_R =55, and (c) D_R=75% with vertical effective stress of 1 P_{atm}, and Ko=0.5

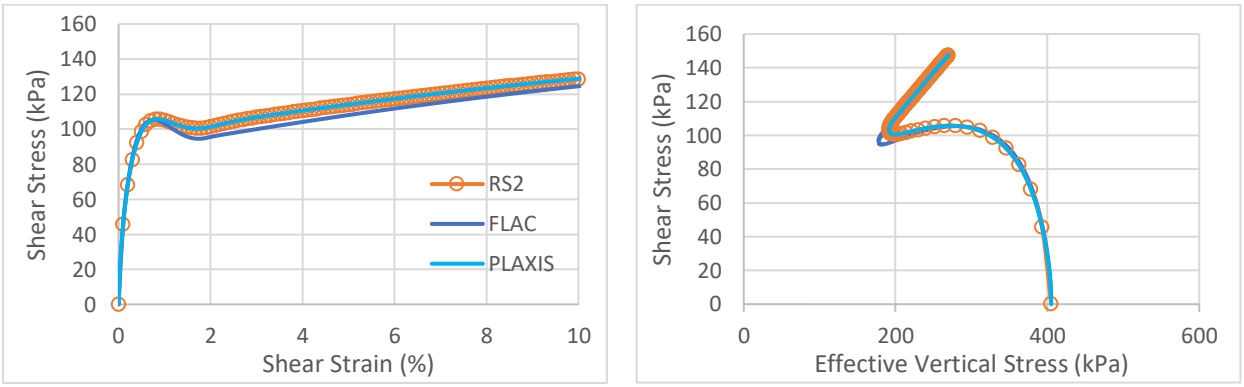

(a)

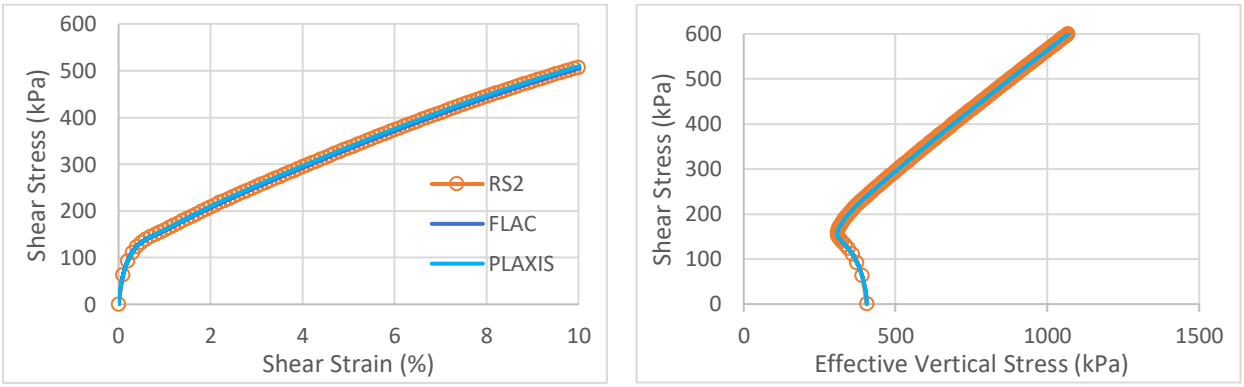

(b)

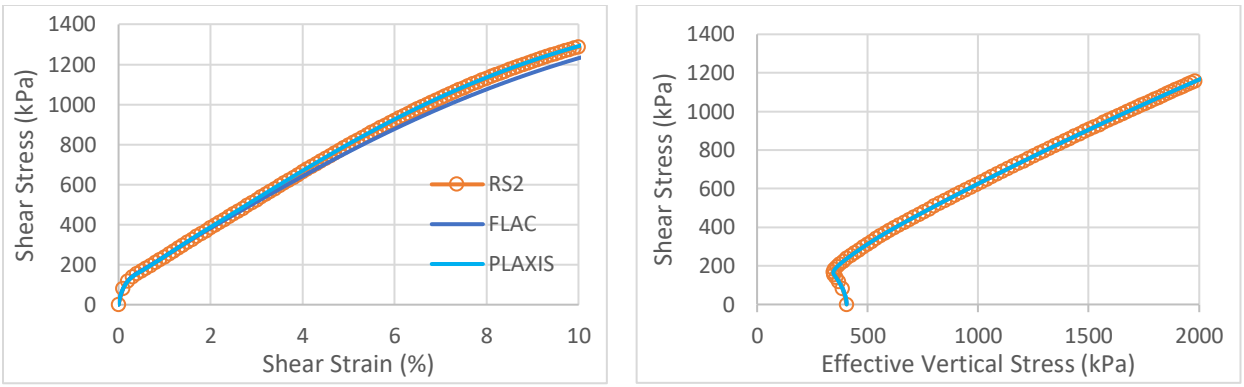

(c)

Figure 3.8. Monotonic Undrained Simple Shear Test loading responses for (a) D_R = 35% (b) D_R =55, and (c) D_R=75% with vertical effective stress of 4 P_{atm}, and Ko=0.5

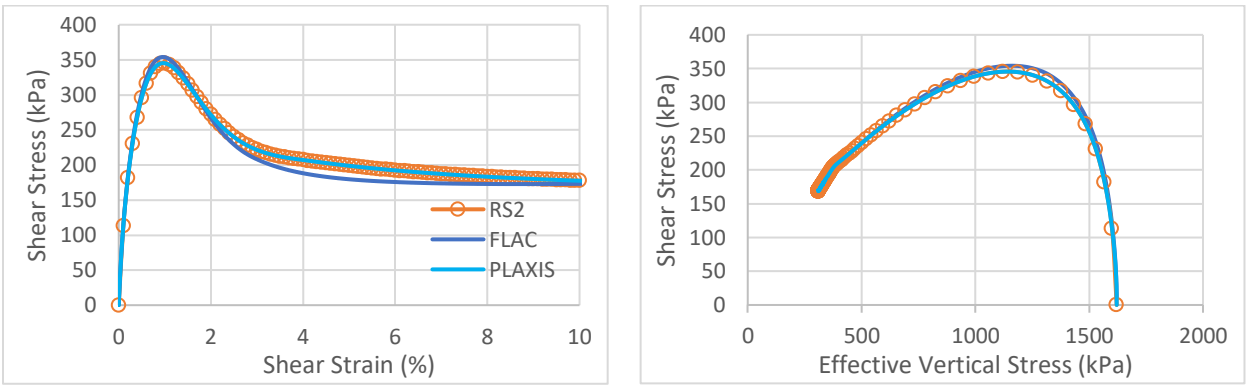

(a)

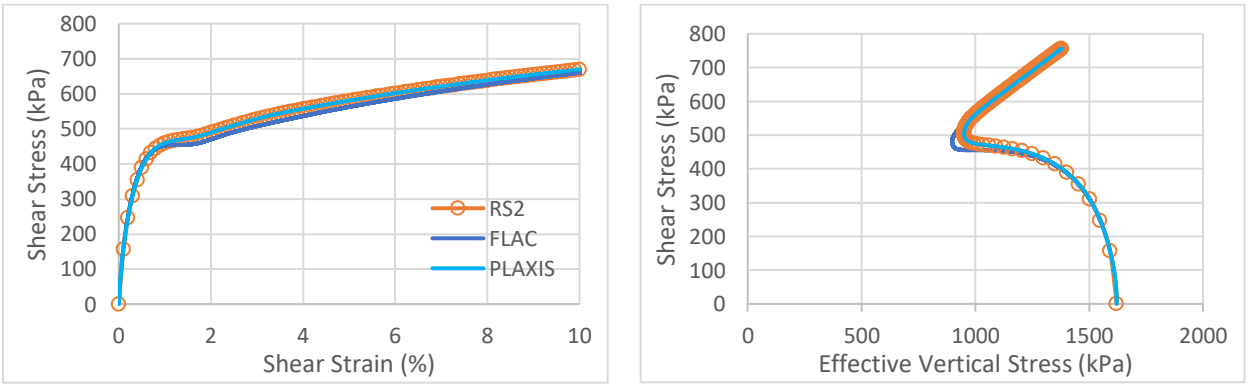

(b)

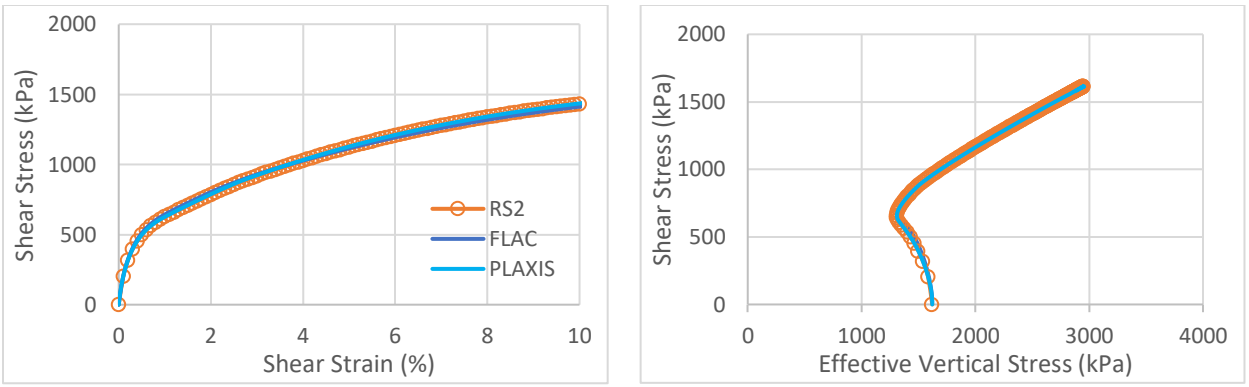

(c)

Figure 3.9. Monotonic Undrained Simple Shear Test loading responses for (a) D_R = 35% (b) D_R =55, and (c) D_R=75% with vertical effective stress of 16 P_{atm}, and Ko=0.5

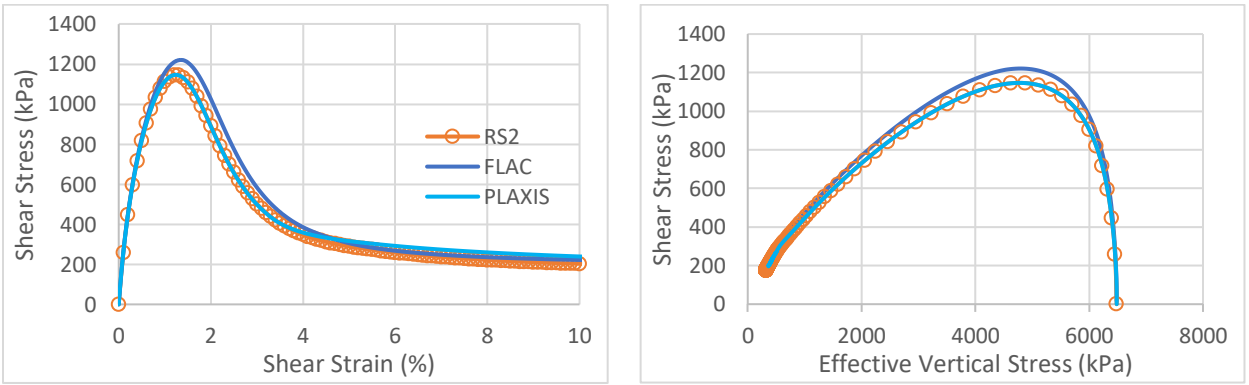

(a)

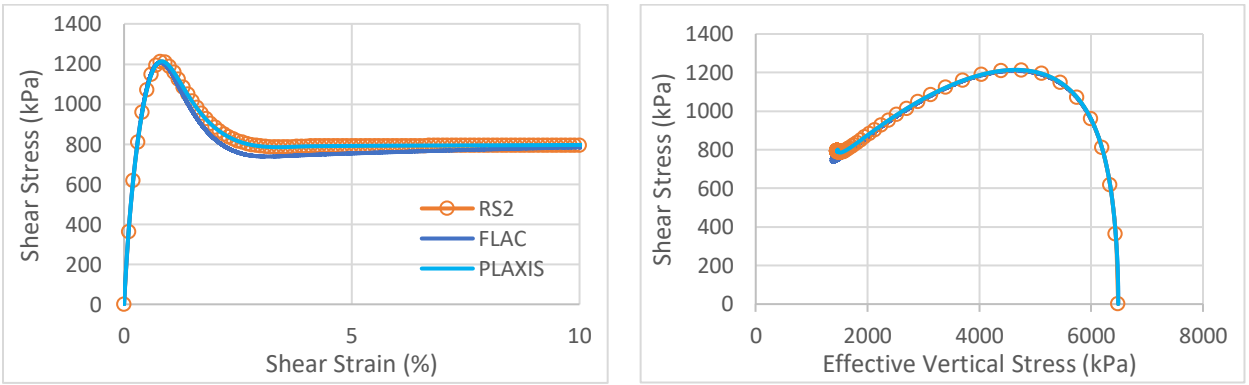

(b)

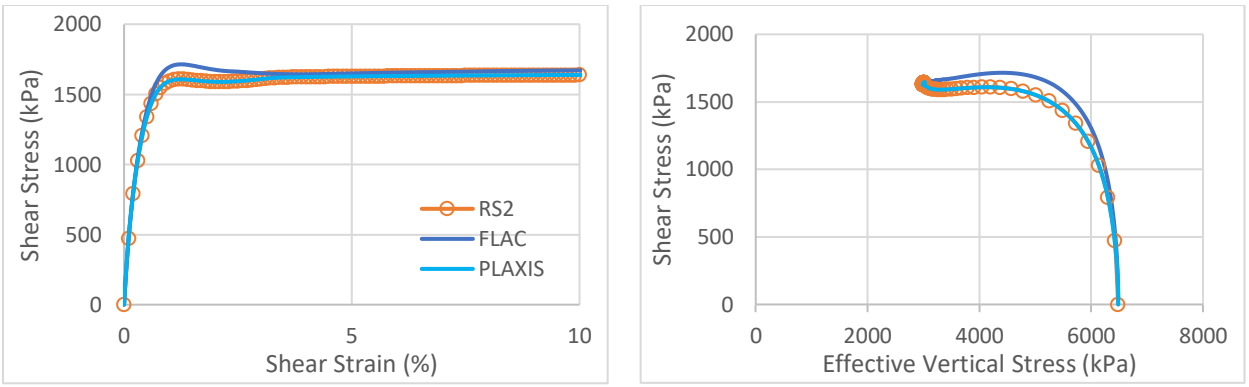

(c)

Figure 3.10. Monotonic Undrained Simple Shear Test loading responses for (a) D_R = 35% (b) D_R =55, and (c) D_R=75% with vertical effective stress of 64 P_{atm}, and Ko=0.5

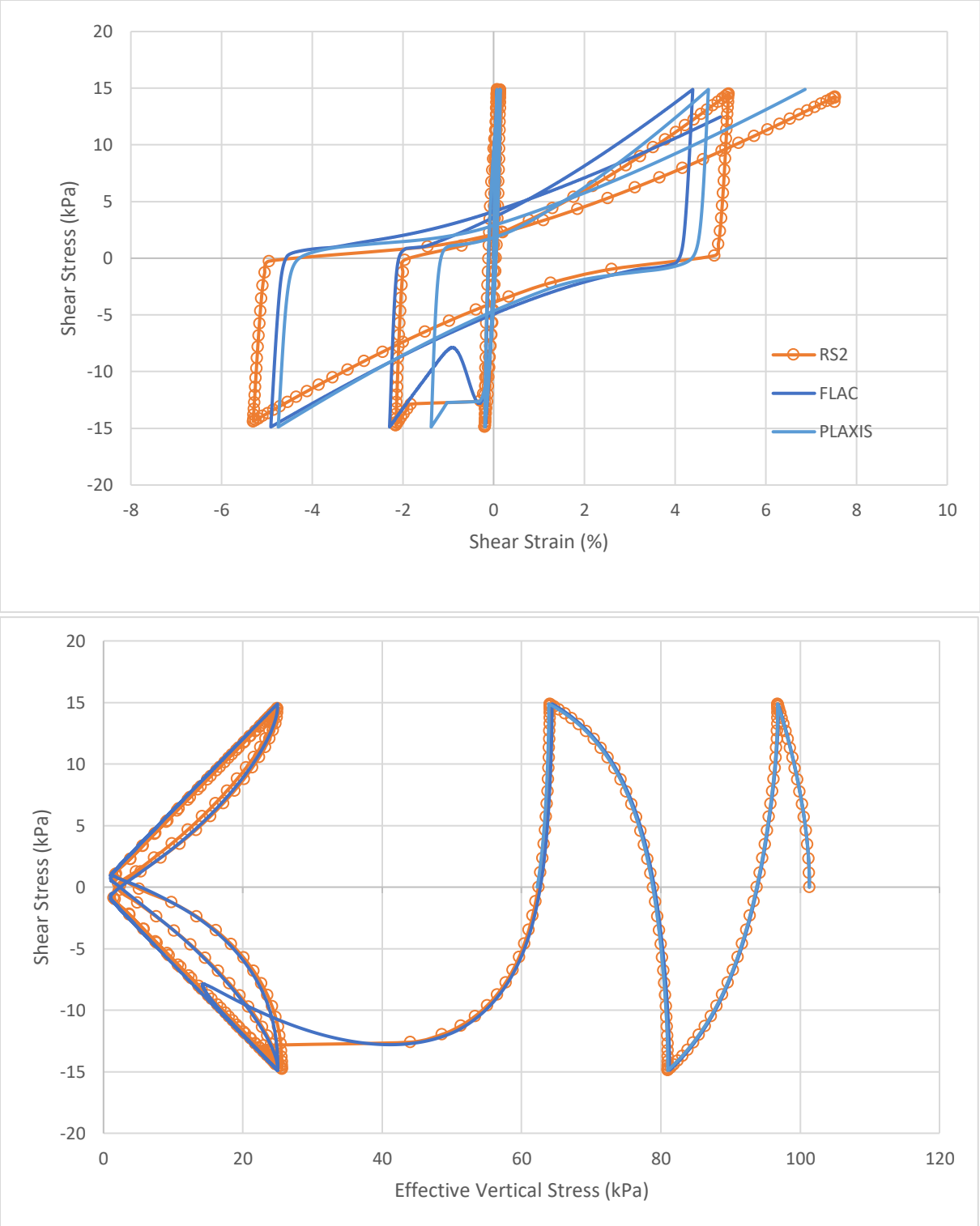

Figure 3.11. Cyclic Undrained Simple Shear Test loading responses for D_R = 35% under vertical effective stress of 1 P_{atm}, and Ko=0.5 with maximum loading ratio of 0.147; (a) variation of share stress with shear strain and (b) effective stress path

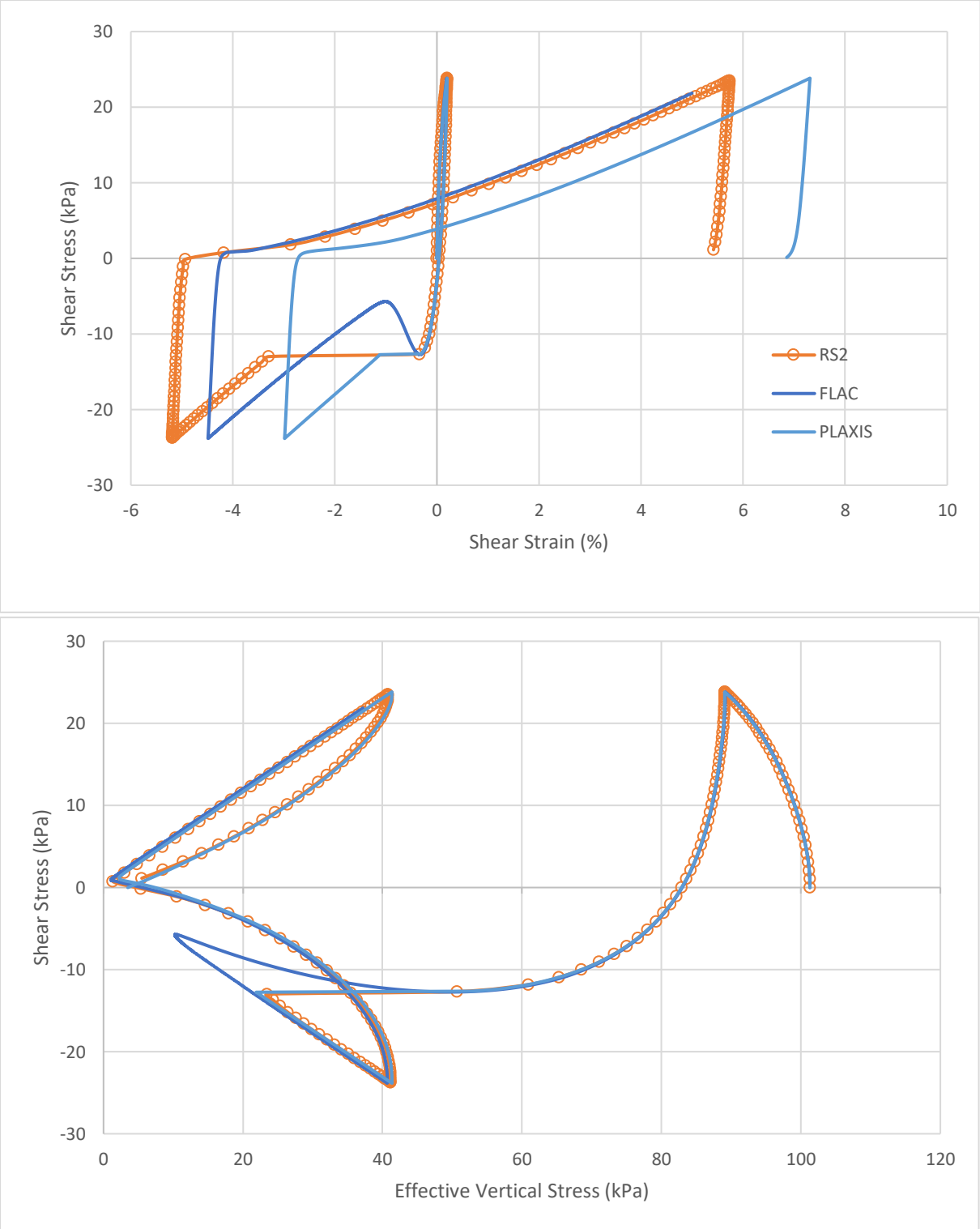

Figure 3.12. Cyclic Undrained Simple Shear Test loading responses for D_R = 35% under vertical effective stress of 1 P_{atm}, and Ko=0.5 with maximum loading ratio of 0.147*1.6; (a) variation of share stress with shear strain and (b) effective stress path

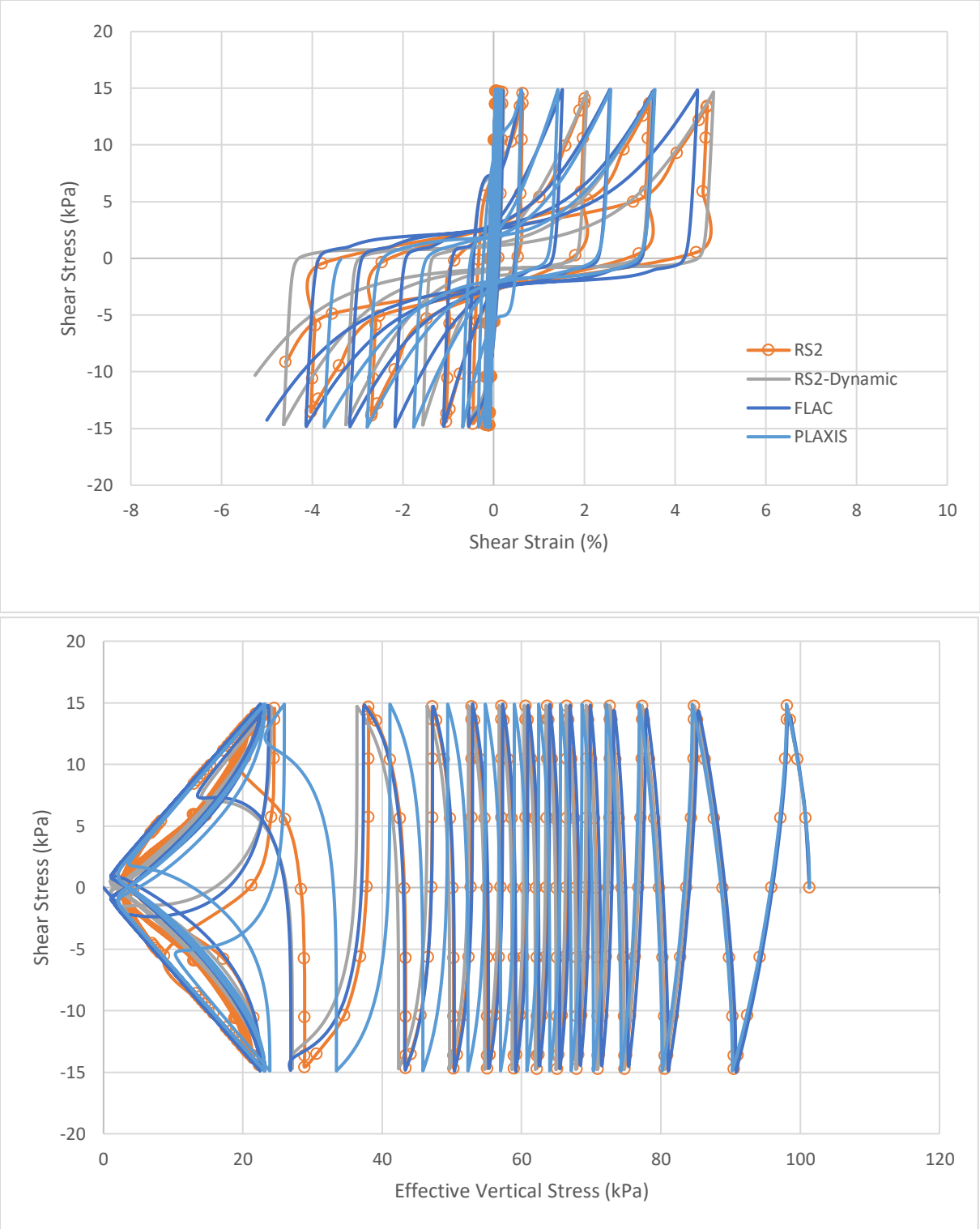

Figure 3.13. Cyclic Undrained Simple Shear Test loading responses for D_R = 55% under vertical effective stress of 1 P_{atm}, and Ko=0.5 with maximum loading ratio of 0.147; (a) variation of share stress with shear strain and (b) effective stress path

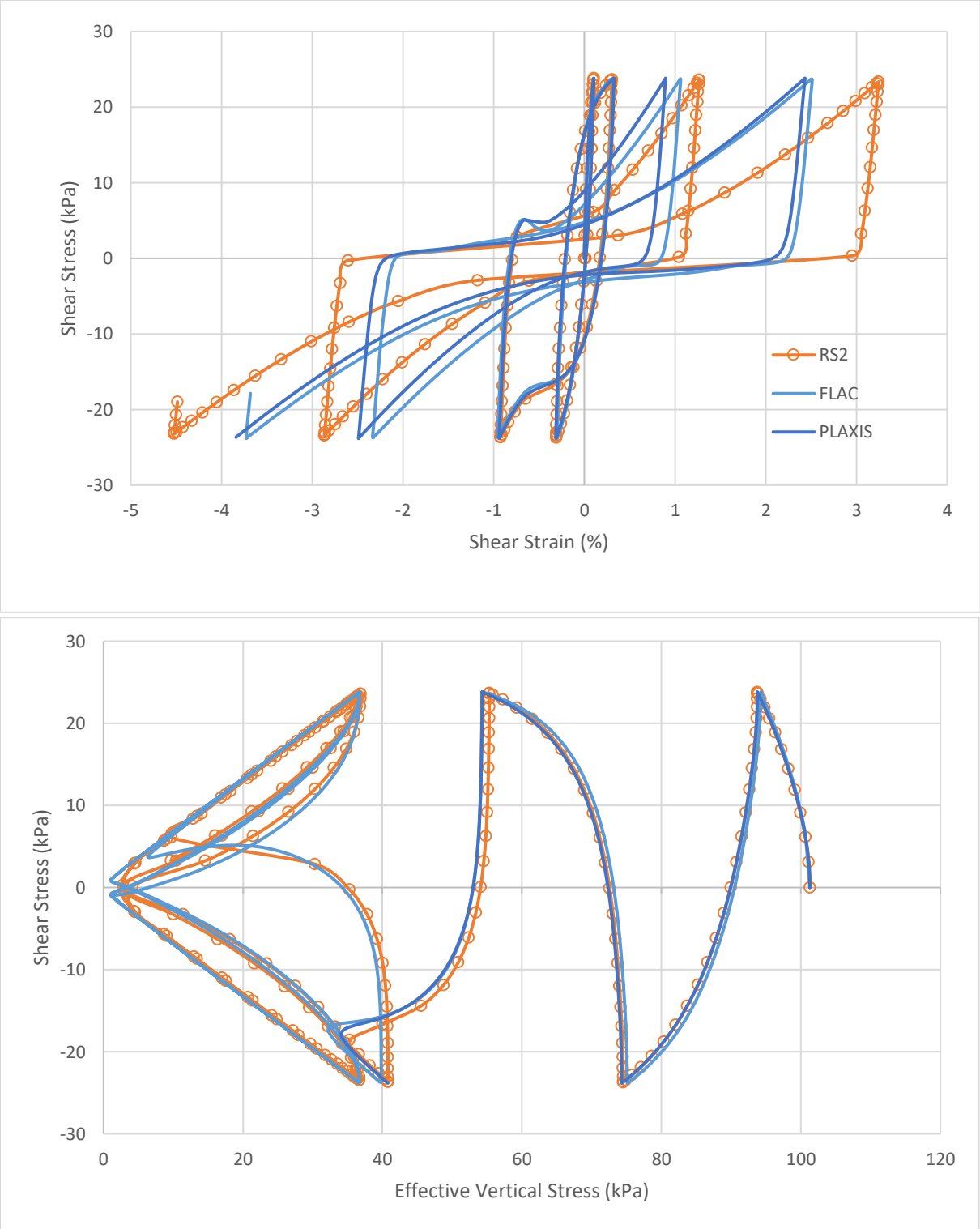

Figure 3.14. Cyclic Undrained Simple Shear Test loading responses for D_R = 55% under vertical effective stress of 1 P_{atm}, and Ko=0.5 with maximum loading ratio of 0.147*1.6; (a) variation of share stress with shear strain and (b) effective stress path

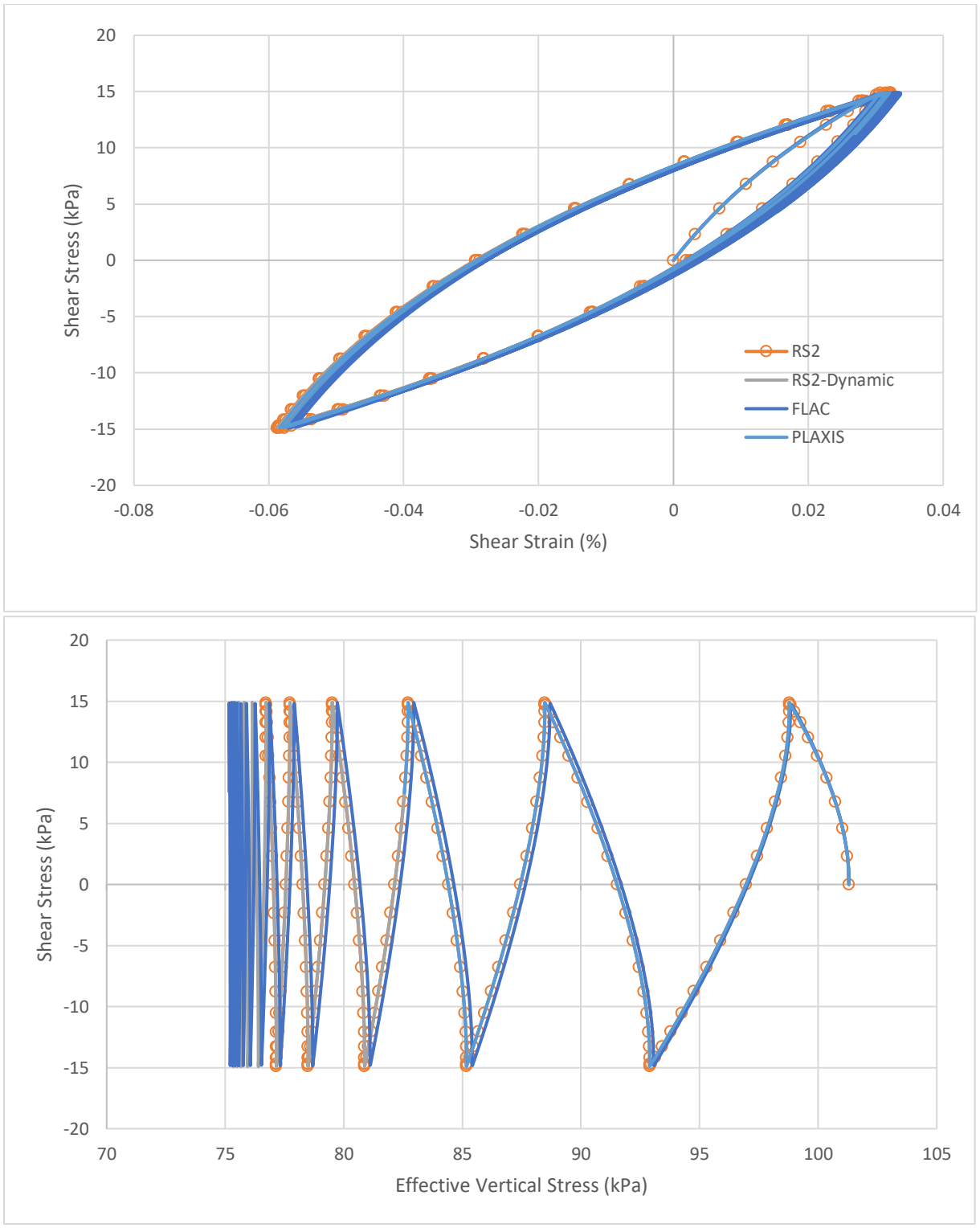

Figure 3.15. Cyclic Undrained Simple Shear Test loading responses for D_R = 55% under vertical effective stress of 1 P_{atm}, and Ko=0.5 with maximum loading ratio of 0.1476; (a) variation of share stress with shear strain and (b) effective stress path

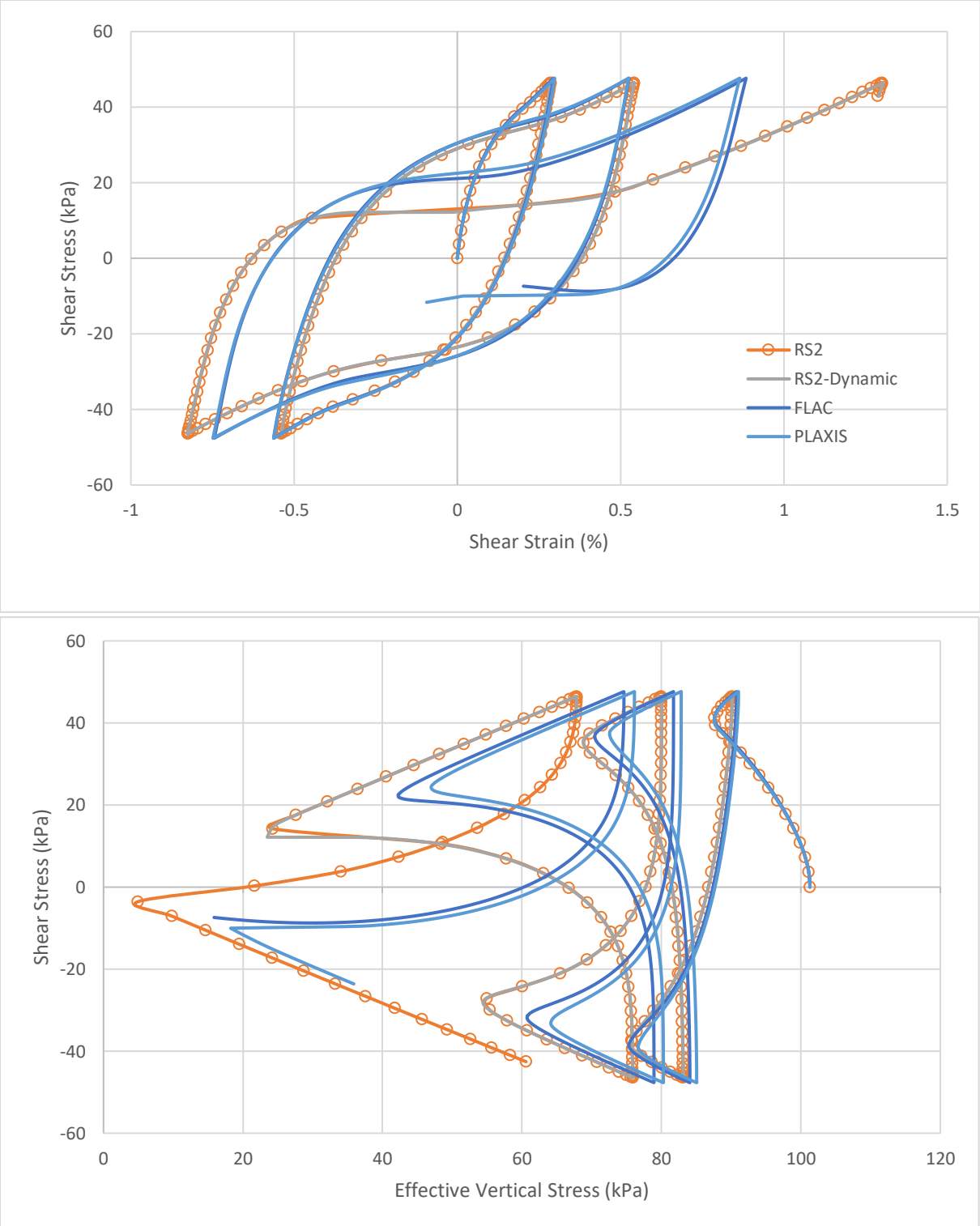

Figure 3.16. Cyclic Undrained Simple Shear Test loading responses for D_R = 55% under vertical effective stress of 1 P_{atm}, and Ko=0.5 with maximum loading ratio of 0.147*3.2; (a) variation of share stress with shear strain and (b) effective stress path

References

Been, K., and Jefferies, M. G. (1985). "A state parameter for sands." Géotechnique 35(2), 99–112.

Boulanger, R. W., & Ziotopoulou, K. (2017). PM4Sand (version 3.1): A sand plasticity model for earthquake engineering applications. Rep. No. UCD/CGM-17/01. Davis, CA: Center for Geotechnical Modeling, Dept. of Civil and Environmental Engineering, Univ. of California.

Dafalias, Y. F., and Manzari, M. T. (2004). "Simple plasticity sand model accounting for fabric change effects." Journal of Engineering Mechanics, ASCE, 130(6), 622-634.

Itasca (2016). FLAC – Fast Lagrangian Analysis of Continua, Version 8.0, Itasca Consulting Group, Inc., Minneapolis, Minnesota.

Kutter, B. L., and Chen, Y.-R. (1997). “Constant p’ and constant volume friction angles are different.” ASTM Geotechnical Testing Journal, ASTM, 20(3), 304-316.

Plaxis, "User’s manual of PLAXIS." (2018).

Yu, P., and Richart, F. E., Jr. (1984). "Stress ratio effects on shear modulus of dry sands." J. Geotechnical Engineering, ASCE, 110(3), 331-345.

Ziotopoulou, K. (2014). "A sand plasticity model for earthquake engineering applications." PhD Dissertation, University of California, Davis.